Journal of Volcanology and Geothermal Research 193 (2010) 67–81

Contents lists available at ScienceDirect

Journal of Volcanology and Geothermal Research

journal homepage: www.elsevier.com/locate/jvolgeores

Infrasound from Tungurahua Volcano 2006–2008: Strombolian to Plinian eruptive activity

David Fee [a,*], Milton Garces [a], Andrea Steffke [b]

[a] Infrasound Laboratory, University of Hawaii at Manoa, 73-4460 Queen Kaahumanu Hwy, #119 Kailua Kona, HI 96740, USA
[b] Hawaii Institute of Geophysics and Planetology, School of Ocean and Earth Science and Technology, University of Hawaii at Manoa, 1680 East-West Road, Honolulu, HI 96822, USA

ARTICLE INFO

Article history:
Received 27 October 2009
Accepted 15 March 2010
Available online 27 March 2010

Keywords:
volcano acoustics
infrasound
jet noise
Tungurahua
Plinian

ABSTRACT

Strombolian to Plinian activity from Tungurahua Volcano, Ecuador has been recorded by the autonomous infrasound arrays of the Acoustic Surveillance for Hazardous Eruptions (ASHE) project since early 2006. Our studies suggest that acoustic energy release during large eruptions does appear to broadly scale with eruption intensity. This manuscript provides a detailed chronology and characterization of Tungurahua's eruptive activity between 2006 and 2008 and demonstrates the ability to constrain source parameters of significant eruptions, such as onset, duration, and escalation, at regional distances by combining infrasound and remote sensing techniques. The ASHE system in Ecuador automatically detected over 20,000 volcanic explosions at an array 37 km from Tungurahua and was successful at notifying the onset, escalation, and cessation of a hazardous February 2008 eruption with a latency of 5 min. Elevated infrasonic energy from sustained and intense Tungurahua eruptions correlates well with ash column heights and their lateral extent during the study period. The spectra of these sustained explosive eruptions appear to be recurrent, readily recognizable, and indicative of volcanic jetting and significant atmospheric ash injection. The paroxysmal Plinian phase of the August 2006 eruption produced an ash cloud that extended well into the stratosphere (>24 km), coinciding with a shift of the dominant jetting frequency from 0.25 Hz to below 0.1 Hz, and radiation of over 5×10^7 W of acoustic power. Transient explosions were often marked by minor or no ash release and are presumed to be more gas-rich. A change in the acoustic spectrum of volcanic jetting was also detected in the transition from a sustained to collapsed eruption column at the end of the July 14, 2006 eruption. The jetting spectrum at Tungurahua during a period of sustained pyroclastic density current production changes from a typical double-peaked to a single-peaked spectrum, suggesting remote acoustic monitoring can help ascertain the stability and dynamics of an eruptive column.

1. Introduction

In early 2006 two infrasound arrays were deployed in Ecuador as part of the proof-of-concept Acoustic Surveillance for Hazardous Eruptions (ASHE) project (Garces et al., 2008) to monitor and mitigate the significant volcanic ash hazard to aviation in this region. The initial goal of the ASHE project was to determine the feasibility of acoustically detecting significant atmospheric ash emissions and rapidly notifying civil defense authorities (ideally, within 5 min). The feasibility study has been successfully completed (Garces et al., 2008), and this paper provides details on the methods, salient scientific results, capabilities, and vulnerabilities of this remote sensing technology.

The Washington, DC Volcanic Ash Advisory Center (VAAC) is responsible for ash monitoring for aviation in this region. Existing seismic (Kumagai et al., 2007), gas (Arellano et al., 2008), satellite (Carn et al., 2008), and other technologies currently monitor Ecuador, but the persistently poor visibility, elevated eruptive activity, and remoteness of the region make the task of detecting ash emissions and notifying the necessary authorities challenging. Low-frequency (<20 Hz) sound waves (infrasound) propagate long distances with little attenuation and are not affected by the dense cloud cover often present in the region. Further, infrasound is a direct measurement of pressure release into the atmosphere, in this case the eruption of pressurized gas, ash, and lava, and is thus a good indicator of explosive volcanic activity. Accurately differentiating and identifying the character of eruptive pressure release at the volcano is the most difficult and crucial aspect.

Between March 2006 and February 2008 near constant and diverse infrasound from Tungurahua Volcano was recorded by the two ASHE arrays. This paper provides a detailed chronology and characterization of the eruptive activity using infrasound and satellite imagery. We expand on the ash monitoring results presented in Garces et al. (2008) and present a companion paper to the satellite-based ash plume

* Corresponding author.
E-mail addresses: dfee@isla.hawaii.edu (D. Fee), milton@isla.hawaii.edu (M. Garces), steffke@higp.hawaii.edu (A. Steffke).

0377-0273/$ – see front matter © 2010 Elsevier B.V. All rights reserved.
doi:10.1016/j.jvolgeores.2010.03.006

observations of Steffke et al. (in review), from which the ash clouds heights and dimensions listed here are derived. We focus on five time periods of volcano-acoustic activity. These periods are representative of a common eruption style and/or significant eruption at Tungurahua thus far observed during the experiment: Strombolian (January 2008), Vulcanian (May 2006, February 2008), Sub-Plinian (July 2006), and Plinian (August 2006). These recordings are noteworthy in that they are some of the highest quality and diverse infrasound measurements of explosive volcanism.

Beyond the monitoring aspect, this manuscript seeks to demonstrate the capability of correlating acoustic records with satellite-derived observations to constrain source mechanisms. For Tungurahua Volcano, we focus on three main aspects: (1) timing: onset, duration, and end of activity; (2) evolution: changes in intensity and character of the signal, in both the time and frequency domain; and (3) source: the physical generation of acoustic energy and how this relates to ash, gas, and pyroclastic density current (PDC) production. The relationship between PDCs and their associated acoustic signals is not currently understood, and this paper provides a unique opportunity to study the infrasound produced from sustained vs. collapsing columns. Further, high quality infrasonic records from energetic silicic eruptions are rare, and this project provides the first detailed, continuous, high fidelity acoustic recordings of all stages of a Plinian eruption.

2. Regional setting and previous work

2.1. Tungurahua Volcano

Tungurahua is one of the most active stratovolcanoes in the Ecuadorian Andes (Fig. 1). At 5023 m, the steep sloped volcano has experienced infrequent but dangerous sector collapses and immense debris flows in its history. Recent activity at the andesitic–dacitic volcano has been characterized by near continuous activity from the central crater in the form of PDCs, lava flows, and ash emissions. Although not located near a major city, over 25,000 residents live in close proximity and within the path of PDCs and lahars (Hall et al., 1999). The numerous ash emissions from Tungurahua pose a threat to regional and international aviation, and during the study period the VAAC issued near daily advisories (sometimes multiple advisories per day) concerning Tungurahua emissions.

After an ~80 year lull, Tungurahua has seen a resurgence of activity since 1998. Seismic activity increased at Tungurahua between September 1998 and 1999, indicating magma rising through the conduit. In October 1999 magma reached the surface and produced Strombolian explosions. Between October 1999 and March 2006 activity alternated between episodes of Strombolian–Vulcanian explosions and lulls characterized by relatively passive degassing in the form of steam or ash emissions (Arellano et al., 2008; Ruiz et al., 2006).

2.2. Previous infrasound studies at Tungurahua

The Ecuadorian Instituto Geofísico de la Escuela Politécnica Nacional (IG) has operated a multiparameter network at Tungurahua since 1988. Several seismo-acoustic studies have been undertaken at Tungurahua. Johnson (2003) found difficulty correlating seismic and acoustic data because of the high level of seismic background tremor. Another deployment focusing on correlating energy release with eruptive plumes (Johnson et al., 2005) found a poor correlation between total acoustic energy release and eventual plume size. The size of the eruptions described in that study are of much lower magnitude than the case studies presented here. Minor jetting signals were recorded in these studies as well. Ruiz et al. (2006) used waveform similarity to classify acoustic explosions into distinct clusters. Seismic–acoustic travel time differences reveal the explosions originated at shallow and variable depths within the conduit. Garces et al. (2008) introduced the ASHE project, preliminary results, and its relation to international infrasonic monitoring systems. Using data from the ASHE arrays, Matoza et al. (2009) showed how the infrasound signals recording during large, sustained eruptions at Tungurahua resemble noise from man-made jets.

3. Materials and methods

3.1. Equipment

Two four element infrasound arrays were deployed with the aim of detecting and differentiating between multiple volcanoes and other infrasonic sources at regional distances. The RIOE array (Fig. 1a) is located 36.75 km southwest of Tungurahua Volcano, 43 km from Sangay Volcano, 214 km from Reventador Volcano, and ~170 km south of Quito, Ecuador. This is the primary array used for this study, as it is the closest to Tungurahua, which is by far the most acoustically active volcano during the study period. The RIOE array aperture is ~150 m. Assuming a sound speed of 340 m/s, the travel time for an

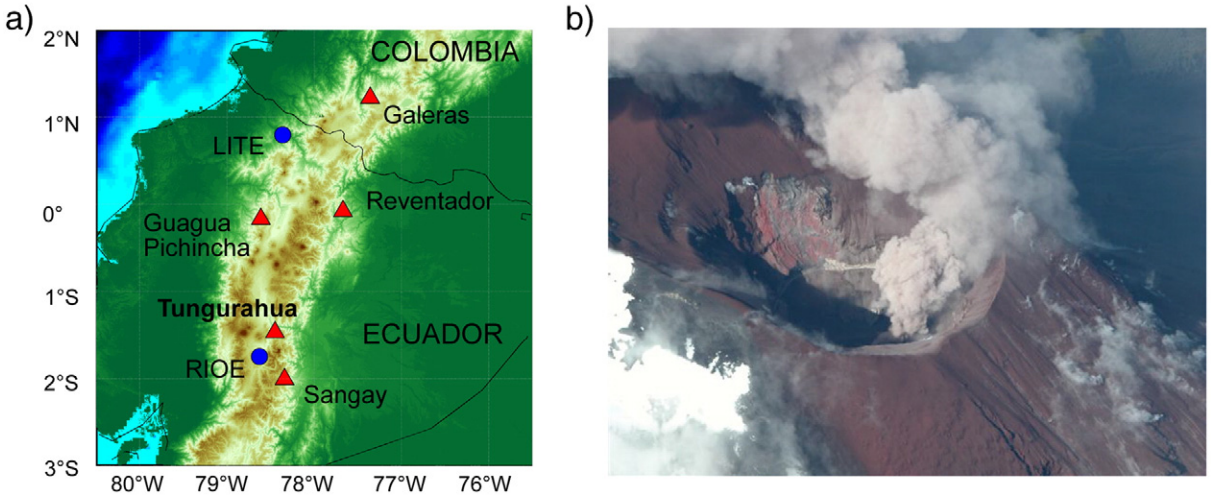

Fig. 1. a) Map of study area. ASHE arrays are denoted as blue diamonds, while acoustically detected volcanoes are denoted by red triangles. This study focuses on the RIOE array and Tungurahua Volcano. b) Photo of the Tungurahua summit crater after the August 16 eruption. The crater width is estimated at 300–400 m and the depth to >100 m. Photo courtesy of Patricio Ramon (IG).

acoustic pulse from Tungurahua to RIOE is ~109 s. Although infrasound from Tungurahua Volcano dominated at RIOE, signals from Sangay, Reventador, and Galeras Volcano, Colombia (359 km) were also detected.

The LITE array (Fig. 1a) is located near the Colombia–Ecuador border, 121 km southwest of Galeras volcano, 124 km from Reventador volcano, and 251 km north of Tungurahua. This location was chosen due to its proximity to Galeras volcano and the predicted first thermospheric acoustic arrival from Tungurahua. The LITE array aperture is ~120 m. During the course of the experiment volcanic signals from Tungurahua, Reventador, Galeras, and Nevado del Huila Volcanoes, Colombia were recorded at LITE.

Chaparral 2.2a microphones were used at both arrays. These sensors have a flat frequency response between 0.1 and 200 Hz and were sampled at 40 Hz. Data were recorded using 24-bit digitizers and sent by satellite to the Geological Survey of Canada, where it was then forwarded on to the University of Hawaii Infrasound Lab. A broadband seismometer was also deployed at each array.

3.2. Remote volcanic monitoring using acoustic arrays

As infrasound technology becomes a more widely used to monitor volcanoes, it is important to realize that site selection is crucial to successful monitoring. This project chose to place the acoustic arrays at a safe distance from the active volcanoes in Ecuador and southern Colombia. One of the main benefits of placing microphones arrays at regional distances (approximately 10–200 km) is that it permits the detection and discrimination of multiple volcanoes, one of the prime objectives of the ASHE project. Background noise levels are frequently lower at regional distances compared to the exposed, high wind locations often found near active volcanoes where infrasound sensors are often deployed. There is also less chance of instrument loss from PDCs and other volcanic hazards near the active vent. Easier access to the site can also be facilitated by placing the equipment further away, decreasing the amount of station downtime. The arrays are located in the far-field (where $kr \gg 1$, with $k = 2\pi \times wavelength$ and $r =$ distance to the source), where the non-linear and hydrodynamic effects associated with high source pressure signals are reduced and the monopole radiation component dominates (Pierce, 1981). This project also benefits from its extended duration and consistency of atmospheric variations (primarily diurnal wind changes). Although latency issues arise for long distances, this project finds that propagation, detection, and notification under 5 min is still feasible for regional deployments within tens of kms of the volcano.

Regional deployments do have their vulnerabilities. Changes in the atmosphere, particularly the diurnal boundary layer and winds in the troposphere, can affect the acoustic signals at these ranges (Fee and Garces, 2007). Scattering from turbulence and other phenomena may also complicate propagation (Pierce, 1981). The higher frequency acoustic signals will also experience more atmospheric absorption ($\sim 10^{-3}$ dB/km at 10 Hz vs. 10^{-6} dB/km at 0.1 Hz) (Sutherland and Bass, 2004), thus the signals at greater distances will be slightly biased towards lower frequency. Further, lower signal levels will be recorded due to geometrical spreading, assumed to be 1/r for RIOE. These vulnerabilities can be minimized by proper site selection and a satisfactory understanding of the atmosphere. Source directionality may also complicate derivation of source parameters for both local and regional deployments (Garces et al., in review).

3.3. Infrasound detection and notification methods

A variety of signal processing techniques are used to detect and identify hazardous volcanic signals. By deploying arrays of sensors rather than single sensors, we can determine the azimuth of coherent acoustic waves as they propagate across the array. This also permits the differentiation between signals of interest, signals that we are not concerned with (termed clutter), and uncorrelated noise. The Progressive Multi-Channel Correlation (PMCC) method (Cansi, 1995) is used to detect signals arriving at each array. For RIOE, PMCC is run for the entire dataset between 0.5 and 4 Hz and split into 10 frequency bands. The 0.5–4 Hz band is where most of the volcanic signals are concentrated. The time segments are split up into 10 second windows with 90% overlap. After PMCC detections are made, they are assigned to "families" based on similar waveform properties. Time-delay beamforming (DeFatta et al., 1998) is used to increase the signal to noise for both the explosion and sustained signal detection. All decibel levels are referenced to 20×10^{-6} Pa.

The ASHE volcanic signal detection system is divided into two main components: explosions and sustained signal (such as tremor and jetting). The acoustic source energy (or acoustic energy) is calculated both for short duration explosions and more sustained sources to determine how energetic the volcanic signal is and how it changes over time. The intensity of an acoustic wave is defined as the average rate of flow of energy through a unit area normal to the direction of propagation, $I = p^2/\rho c$, where p is the excess pressure. The total net outflow (flux) of acoustic energy through a surface is the integral of intensity over the surface. The total acoustic energy can be calculated by integrating the intensity over time and over the surface through which it passes (Pierce, 1981). For a spherical source radiating sound into free space, represented by a sphere with surface area $4\pi r^2$, the acoustic energy can be estimated by:

$$E_a = \frac{4\pi r^2}{\rho c} \int_0^T \Delta p^2(t) dt \quad (1)$$

where $r =$ source–receiver distance, $\rho =$ air density, $c =$ sound speed, and $\Delta p =$ change in pressure. If a hemispherical acoustic source is located on a flat surface, or the source is buried and radiates through an open vent, the source energy radiates into a hemispherical volume and the surface area is reduced by 1/2 to $2\pi r^2$, reducing Eq. (1) by a factor of two. This assumption has been used to estimate the acoustic energy from some volcanoes (Johnson, 2003; Marchetti et al., 2009; Petersen et al., 2006; Vergniolle et al., 1996). However, if the source is just above a surface, in this case a volcanic vent floor, a portion of the source energy radiating isotropically would be reflected back to the atmosphere. For a source placed above a flat, rigid boundary, the acoustic pressure is doubled through reflection (a factor of four in energy) but the total area is halved (Garces et al., in review; Pierce, 1981), adding a net factor of two to Eq. (1). In this study we calculate the acoustic energy using Eq. (1), the mean between a buried and subaerial source. This may underestimate the energy for sources above the vent (such as jetting), but would overestimate surface and subsurface sources (e.g. explosions) by 3 dB, which is well within measurable field accuracy.

Several caveats must be noted in the acoustic energy calculation. First, it assumes the change in pressure (Δp) is entirely produced by the source of interest, and does not account for contributions from noise or clutter. These unwanted contributors can often dominate, particularly in the far-field or during noisy periods. To minimize the effects of wind noise (the dominant noise source), the acoustic energy here is calculated above 0.5 Hz for automatic processing (also removing contamination from the microbarom signal) and above 0.1 Hz for the high signal-to-noise (S/N) case studies selected here. Note the calculation is thus band-limited as well. In addition, the acoustic energy is only calculated if the array processing results yield coherent acoustic signal arriving from within $\pm 7°$ of Tungurahua (26°–40° from RIOE). Eq. (1) also assumes that the source is isotropic and is in a homogeneous space. The complex and dynamic nature of volcanic fluids and pressure release may lead to anisotropic sources, and even relatively simple volcano-acoustic sources have been suggested to be anisotropic (Johnson et al., 2008). However, calculating the radiation patterns from volcano-acoustic sources is

very difficult without proper azimuthal and range sampling. The spherical spreading assumption in Eq. (1) may also be inaccurate, as the RIOE station is located within the diffraction zone and nocturnal ducts and other atmospheric effects may affect transmission loss (Fee and Garces, 2007; Waxler et al., 2008). Due to the aforementioned uncertainties and assumptions made in acoustic energy estimates, comparing acoustic energies between different sources and volcanoes must be taken with care. The technique is best used on a comparison basis for single stations and similar atmospheric conditions.

Using the aforementioned method the acoustic energy for Tungurahua was estimated at 5 minute increments for the preceding hour. As an example, Fig. 2 shows the hourly acoustic energy for on May 12, 2006 0900–1000 UTC. If a high level of hourly acoustic energy is detected, then a notification email is sent to the VAAC and other interested parties. An acoustic source energy of 1×10^8 J over 1 h is the selected notification threshold. If the energy level doubles during the next 5 minute iteration, another notification is sent out. Once the energy level drops below the threshold value, a final email notification is sent.

Many of the signals recorded during the experiment are sustained over an extended period of time. In order to provide a time-relative measure of the volcano's activity, the acoustic energy is converted to acoustic power by dividing the energy value by the time interval. This is most appropriate for continuous processes, such as tremor and jetting (Garces et al., in review). If not otherwise noted, the acoustic power levels quoted here are calculated over 15 minute time intervals. The units of acoustic power are watts (W), and are often denoted as megawatts (MW) or 10^6 W in this manuscript. Unless otherwise stated, all energy values are estimated in the frequency band between 0.1 and 4 Hz.

The explosion detection algorithm for Tungurahua initially high-pass filters the data above 0.5 Hz and runs a STA/LTA (Short term average/Long term average) to determine the onset and end time of any impulsive signal. Two STA/LTA ratios are used, 2/5 and 3/40 s, to ensure both impulsive and somewhat more emergent explosions are detected. Next the explosion must be recorded on all four channels, from which it is then associated with the PMCC detections to ensure the signal is arriving from an azimuth within $\pm7°$ of Tungurahua. The coinciding PMCC family must have a minimum RMS amplitude >0.02 Pa and family size >15 frequency/time bins. If these conditions are met, then an explosion is registered and the time, duration, maximum pressure (P_p), and acoustic source energy are recorded. The acoustic source energy is calculated for the explosion duration, and is then normalized by the energy of a reference event to produce the energy ratio (E_r). The reference event is selected from the beginning of the experiment, Feb. 14, 2006, and has a peak-to-peak amplitude of ~1 Pa and source energy of 1.19×10^7 J. The reference event represents a moderate explosion that is unambiguously detected at RIOE. The explosive acoustic energy is normalized to minimize source geometry, propagation, and topographical effects. Once the algorithms were operational, all explosions with $E_r>5$ triggered a notification email to the VAAC.

3.4. Infrasound monitoring limitations

During periods of low activity or high noise, the infrasound S/N levels are such that the employed algorithms are not as effective in detecting volcanic activity. Since the arrays have insufficient wind noise shelter, the recordings during the middle of the day (~5 h corresponding to ~1700–2200 UTC) are often overwhelmed with wind noise and are not useful for detecting low-level signals. However, during moderate–large explosions (>3 Pa at RIOE) and the three large eruptions (July '06, August '06, and Feb. '08), signal levels were high enough to overcome the ambient wind noise during the middle of the day. More regular maintenance of the arrays would also help raise the detection thresholds by assuring sensor and site responses did not vary.

False detection and classification of volcanic signals is fairly minimal, as the algorithms employed were correlated extensively with volcanological observations in case studies before notification services were initiated. Thunder is one potential source of false detection and notification. A thunderstorm between RIOE and Tungurahua was misidentified as a group of explosions from Tungurahua due to the shared impulsive and transitory nature of both processes. No obvious tremor misidentifications were made, but the possibility cannot be completely ruled out. The low number of false detections can be partially attributed to the exhaustive and detailed monitoring of Tungurahua Volcano by the IG.

At greater distances (e.g. 200 km or more) seasonal changes in wind conditions, particularly at higher latitudes, may affect the detectability of infrasonic signals (Le Pichon et al., 2009). Preliminary analysis shows that acoustic signals from Tungurahua recorded at LITE likely propagate through the thermosphere, and because of the low latitude and north–south propagation path, are not substantially affected by the seasonal variations in stratospheric winds. For stations at higher latitudes, such as the ASHE arrays at Mount St. Helens, USA (~45°N) (Matoza et al., 2007), longer range detection will be influenced more by stratospheric east–west wind variations.

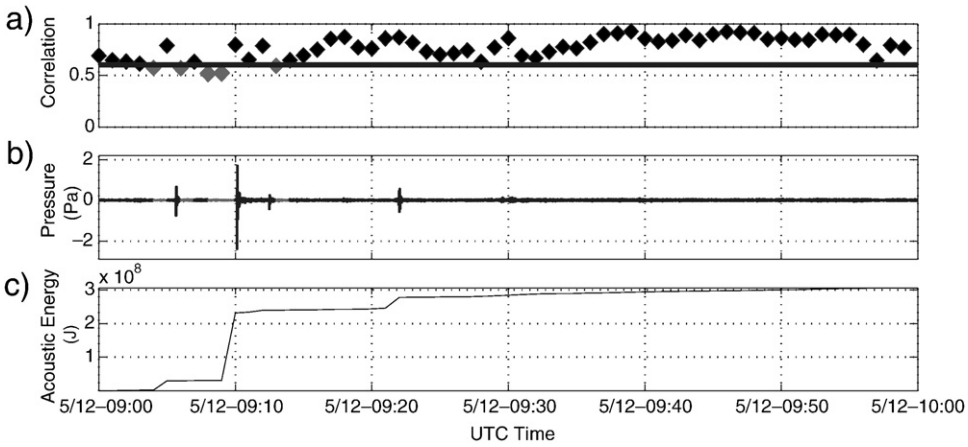

Fig. 2. Typical hourly acoustic energy calculation. RIOE infrasound array data is band-pass filtered between 0.5 and 4 Hz and split into 10 s windows. a) Waveform cross-correlation between the sensors for the time window. Values above 0.6 (black) with azimuths within $\pm7°$ from Tungurahua are selected, while gray segments are either unwanted signal or noise. b) Filtered waveforms, with coherent segments colored black. c) Cumulative acoustic source energy for each coherent segment.

Large explosions can bias the acoustic energy/power calculations, and a more effective way of separating explosions and tremor levels would be helpful. However, the relationship between explosions, tremor, and ash production is complex and not fully understood. For example, large explosions followed by harmonic, gliding tremor may be representative of gas-rich, ash-poor eruptions (e.g. Sections 4.2 and 4.5), and multiple episodes of jetting are preceded (and possibly initiated) by large explosions (e.g. towards the end of the February 6, 2008 eruption, onset of July 14, 2006 eruption, and around 0435 on August 17, 2006).

4. Results

4.1. Experiment results

Between March 2006 and February 2008, 19,865 explosions were detected at RIOE, with over 3500 of those detected at LITE as well. The peak pressures of these explosions at RIOE range from 0.03 to 24.43 Pa (Fig. 3a). The largest explosion saturated the sensors (>25 Pa) on July 17, 2006, and thus is even more energetic. Assuming spherical spreading, this correlates to a peak pressure of over 900 kPa at the vent and is comparable to some of the largest explosions recorded to date by infrasound microphones at near or regional distances Fig. 3 shows both the raw amplitude of each explosion and number of explosions detected per day. Approximately 99% of the explosions are less than 5 Pa. The number of explosions per day ranged from 0 to a peak of 443 on January 25, 2008, which was characterized by energetic Strombolian activity (Vergniolle and Mangan, 2000).

For much of the period, background volcanic activity is characterized by minor ash emissions and a dominant tremor frequency of 1.4 Hz (Garces et al., 2008). The 1.4 Hz tremor is characteristic of relatively passive degassing and minor ash emissions. Explosions are interspersed with the 1.4 Hz tremor and show no obvious correlation. Numerous instances of energetic volcanic jet noise are recorded as well (Matoza et al., 2009), and they all occur during the three large eruption sequences (Feb. 2008, July and August 2006) that will be covered in subsequent sections.

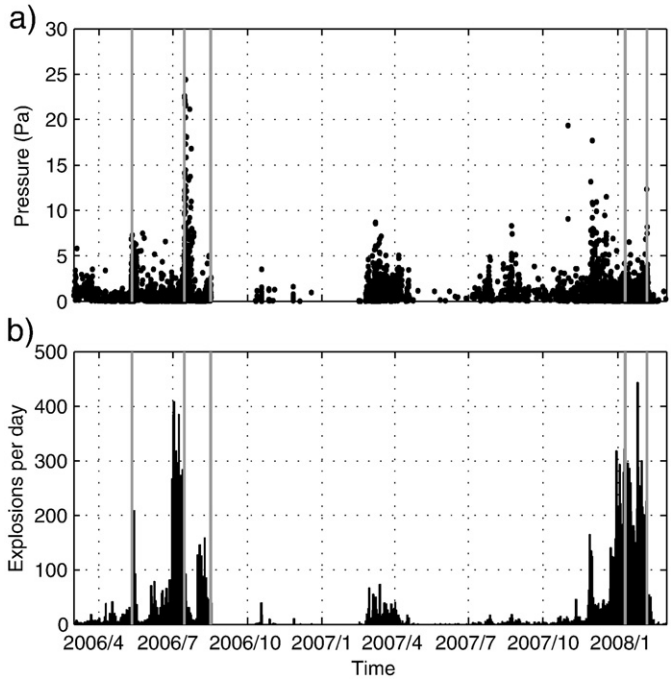

Fig. 3. Tungurahua explosions detected at RIOE. a) Raw pressure amplitude (P_p) and b) numbers of explosions per day. The gray lines indicate times of the case studies selected here.

Coherent acoustic energy from Tungurahua is detected at RIOE during most of the experiment. Fig. 4 shows the hourly coherent acoustic source energy at RIOE divided into three categories: low (10^5–10^7 J), moderate (10^7–10^9 J) and high (>10^9 J). The July 2006, August 2006, and Feb. 2008 eruptions all have sustained acoustic energy above 10^9 J/h (~2.8 MW). Other instances of high acoustic energy are from numerous or large explosions within the hour. Lower level activity is characterized by minor ash emissions associated with the 1.4 Hz tremor and intermittent Strombolian explosions.

Five case studies are now presented in detail, with an emphasis on the acoustic recordings at station RIOE. Each period represents either a large eruption or is typical of a common eruption style at Tungurahua Volcano during the study period. All of the ash plume observations here are derived in Steffke et al. (in review) and are only briefly mentioned here. All times listed are in UTC and ash heights listed are elevation above sea level.

4.2. May 11–15, 2006

In mid-May 2006, eruptive activity increased at Tungurahua Volcano to levels not seen since October 1999. Seismic events began to focus at shallow (0–4 km) depths in April and early May. On May 11 the number of explosions and long period (LP) seismic events increased dramatically (Smithsonian Institution, 2006). Activity remained elevated over the next 5 days and was characterized by large explosions with little ash. May 12 is selected as a case study as it has the most cloud-free satellite images for this period and contained significant acoustic activity. Activity between May 11 and 15 is similar to the 12th. Fig. 5 shows the raw waveforms (a), spectrogram (b), and detected explosions and acoustic power (c) for May 12, 2006.

On May 12, 2006, ninety-seven explosions were detected at RIOE, with 37 having an E_r>1. Some of these explosions were heard in nearby towns almost 30 km from Tungurahua. Moderate to strong explosions occurred regularly throughout the day, with the largest explosion having a peak pressure of 7.8 Pa (Fig. 5a) at RIOE (~287 kPa at the source) and $E_r = 21.5$. Time-averaged 15 minute power levels of sustained activity ranged between ~0.2 and 1.2 MW (Fig. 5c). Most of the acoustic power is due to explosions, not sustained tremor (Fig. 5a). Despite the energetic acoustic activity, no ash plumes are detected in satellite imagery. Discrete volcanic explosions can produce instantaneous plumes, or thermals, if the explosion is short relative to the plume ascent time (Sparks et al., 1997). The IG reported nearly all of the May 12 explosions, but the associated emissions either have low ash content or are comprised primarily of steam and some gas. Some of the explosions ejected incandescent blocks. No thermals were detected by the IG either. The explosive sources for these events are clearly well-connected to the atmosphere and have significant overpressure. Activity during this period is best described as Strombolian.

The 1.4 Hz background tremor was at low levels and fairly constant throughout the day (Fig. 5b). However, the most prominent tremor has a dominant peak below 1 Hz, exhibits gliding (frequency shifting of the spectral peaks) (Fig. 6), and is frequently preceded by large explosions. The gliding tremor is relatively rare in the dataset.

The activity of May 12 was unusual in that the energetic explosions and tremor produced little ash. Examining the waveform features for the May 12 explosions shows they exhibit a high degree of similarity. Most of the explosions are characterized by an impulsive compressional phase, average durations of 7 s, and an often complex rarefaction phase (Fig. 7a). To quantitatively evaluate the similarity of the explosions, basic waveform cross-correlation was performed on all 35 selected explosions for this day following methods similar to that of Green and Neuberg (2006). Explosions with E_r>0.4 were selected, then beamformed, filtered between 0.1 and 10 Hz, and cross-correlated against the master waveform. Fig. 7a shows the explosion waveforms (gray) and master (black), and stacked waveform for all

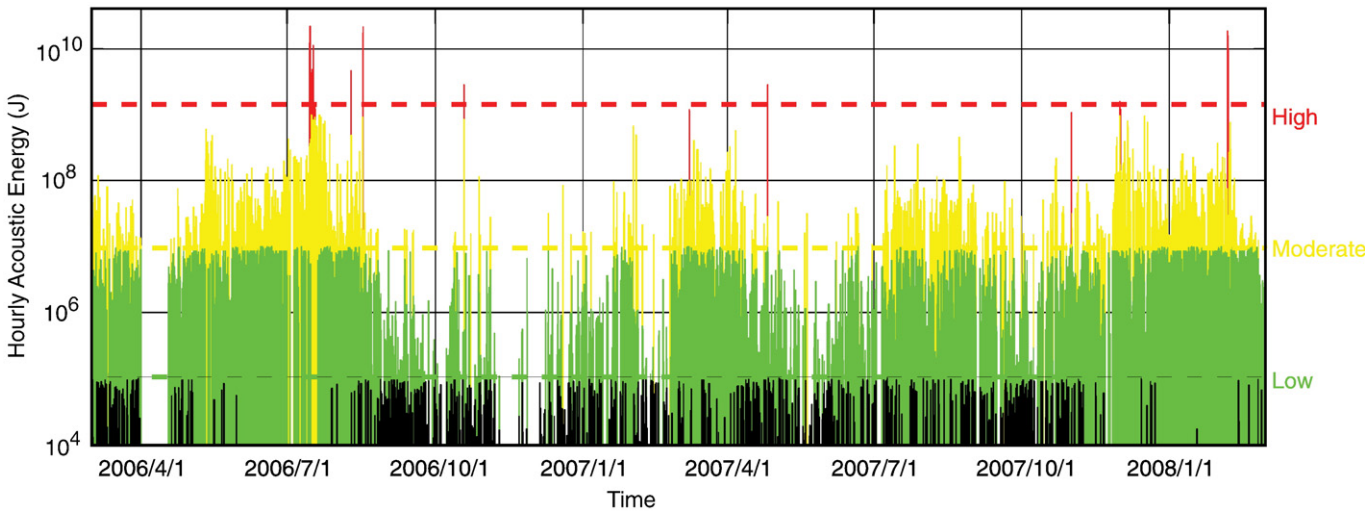

Fig. 4. Hourly acoustic source energy for the experiment. The energy values are split into three levels: low (green) between 10^5 and 10^7 J; moderate (yellow) between 10^7 and 10^9; and high (red) above 10^9 J. Dashed, colored horizontal lines indicate the three threshold energy levels.

the selected explosions (white), while Fig. 7b shows the cross-correlation values between each explosion relative to the master. All of the explosions have high cross-correlation values above 0.75, and most are above 0.9, indicative of similar source processes and minimal changes in propagation induced effects for the selected waveforms. Cross-correlation of the May 12, 2006 master with explosions prior to the July 2006 eruption shows a decrease in the correlation value (~<0.75), as these waveforms have different features.

It is conceivable that a "master" waveform representative of this type of explosion could be constructed and used in a detection algorithm. For example, the explosion detection algorithm could cross-correlate the newly detected waveform against a "master" ash-poor explosion waveform to determine if the new explosion constituted an ash hazard. However, before this could be done a comprehensive waveform cross-correlation study would have to be performed to determine the reliability of this type of test. Neural

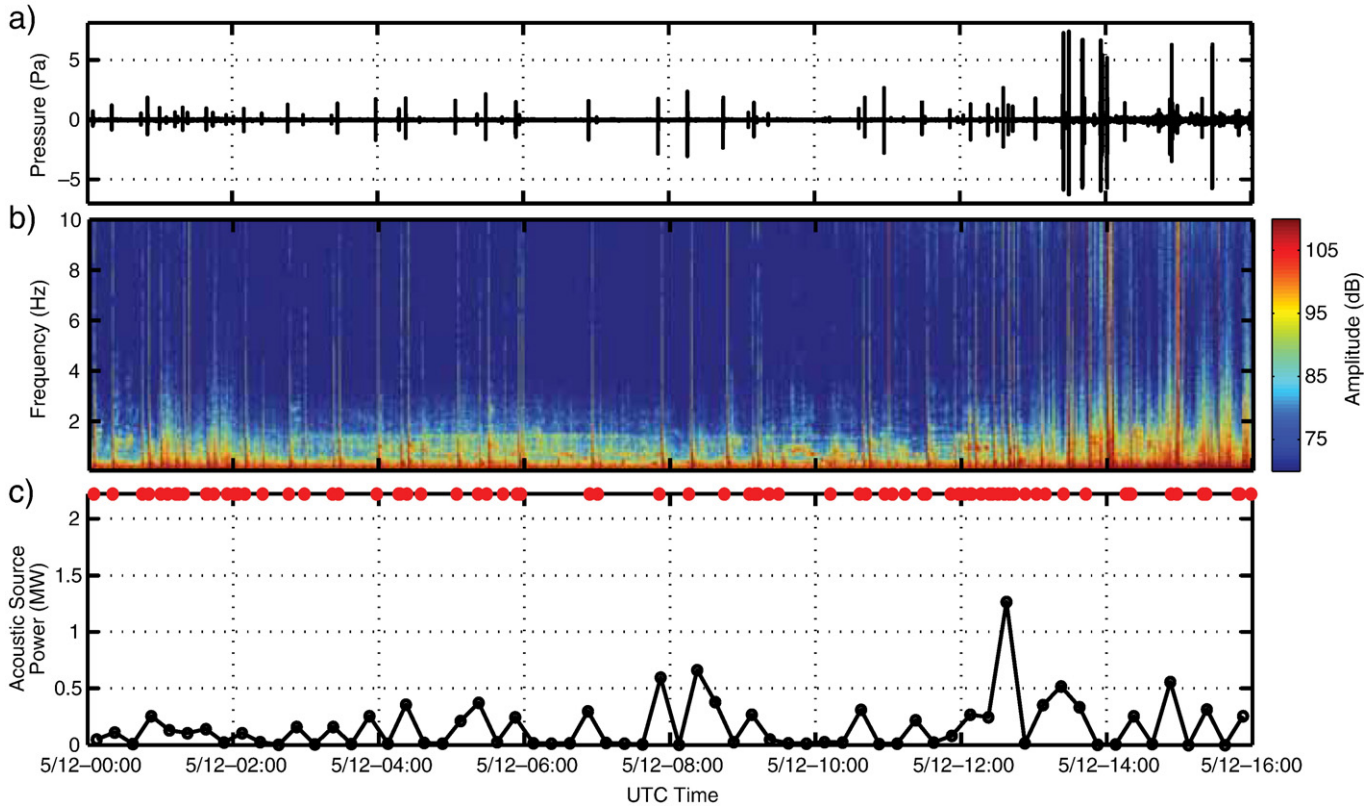

Fig. 5. May 12, 2006 a) raw (unfiltered) beamformed waveform, b) spectrogram, and c) acoustic power (black line) and detected explosions (red dots). Numerous energetic explosions were detected through the day, but no ash plumes were detected in the satellite imagery. Decibel levels for the PSD and spectrograms are referenced to 20×10^{-6} Pa/Hz$^{1/2}$ and are not range corrected. Assuming spherical spreading, the transmission loss at 37 km is 91 dB. All spectrograms and PSD in this manuscript use the same convention.

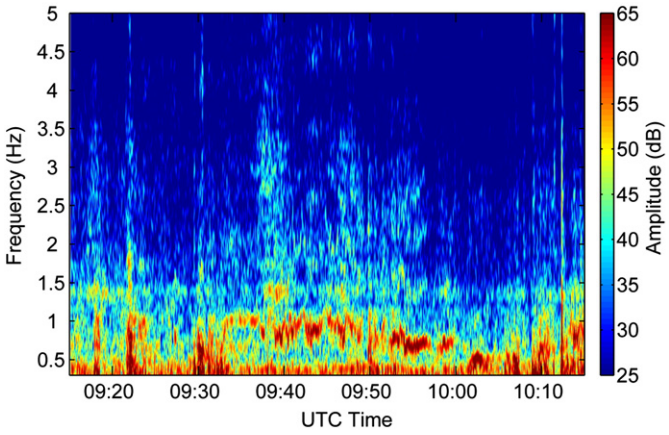

Fig. 6. May 12, 2006 0915–1015 UTC spectrogram between 0.3 and 5 Hz. Explosions during this time period are followed by harmonic, gliding tremor. Background 1.4 Hz tremor is also intermittently present.

network identifiers (e.g. Ham et al., 1999) or other waveform similarity methods (Ruiz et al., 2006) may also be appropriate. It is unclear whether the majority of ash-poor explosions at Tungurahua always have similar waveform characteristics to those of May 12, 2006. This question is beyond the scope of the current study.

4.3. July 14–15, 2006

On July 14–15, 2006 a destructive Subplinian eruption occurred at Tungurahua producing numerous pyroclastic flows and a substantial ash cloud to ~14 km. The eruption had an estimated dense rock equivalent (DRE) volume of magma of ~10^6 m^3 (Arellano et al., 2008) and a total SO_2 discharge of ~12,000 tons (Carn et al., 2008). We estimate the VEI at 3 from the ash cloud heights and duration. In the days preceding the eruption only minor increases in explosive activity occurred (Smithsonian, 2006). Fig. 8 shows the filtered waveforms (a), spectrogram (b), and acoustic power and ash height (c) for the July 15 eruption.

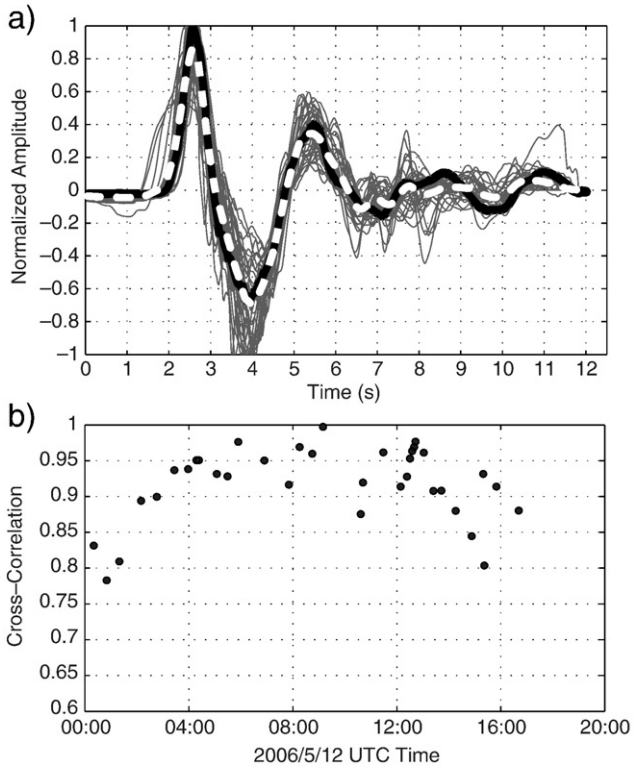

Fig. 7. May 12, 2006 a) waveform and b) cross-correlation results. Explosions with $E_r > 0.4$ are selected and time aligned in a). The black line denotes the master waveform, while the dotted white line indicates the stack of all the waveforms. Each waveform is cross-correlated against the master with the correlation value in b). Most waveforms are highly correlated with correlation values above 0.9.

A moderate explosion occurs on July 14 2234 and signaled the onset of the major eruption. This Vulcanian explosion most likely cleared the conduit and is coincident with the onset of magma fragmentation and ash emissions. Jetting follows the explosion and acoustic power slowly rises from 1 to 2.2 MW by 2345. This is the first instance of intense volcanic jetting recorded at Tungurahua during the experiment. The first satellite imaged ash cloud occurs at 2245 with a height of ~6 km. The plume increases laterally between 2245 and 2345 and rises to ~13.5 km. The first PDC was reported at 2315 (Barba et al., 2006), but no distinctive PDC-related infrasound signal is obvious in our records, likely due to the energetic jetting overpowering the PDC signal. Between 2345 and 0045 a large increase in the plume intensity and lateral extent is observed, and the infrasound power levels rise from ~2.2 to 4 MW. Another large explosion occurs at July 15 0011 ($P_p = 5.31$ Pa, $E_r = 5.19$).

Between 0045 and 0130 UTC the jetting energy is focused at lower frequencies (<1–2 Hz) and infrasound power levels rise rapidly to 9.3 MW. However, no major change in plume height is evident in satellite imagery. The plume reaches a height near its maximum by 0045, although the infrasonic power levels continue to rise until around 0130 and then decrease for ~30 min, only to rise again to a peak of 9.8 MW between 0215 and 0230 (Fig. 8c). These unsteady oscillations in acoustic energy may be typical of sustained jets. Although there is no observable major change in the ash column height associated with the rises in acoustic power between ~0100 and 0230, the maximum lateral extent of buoyant ash cloud occurs around 0230–0330. A large circular plume attached to the vent is apparent in the satellite imagery at 0215 (Fig. 4 in Steffke et al., in review). Because the plume has a high aspect ratio (circular), it is likely that gravitational settling, not wind, is the dominant dispersal mechanism. It is also possible that the ash height peak does not coincide with the maximum acoustic power due to atmospheric effects. The tropopause is located between 16 and 17 km above Tungurahua and could serve as a deterrent to the rising ash cloud due to the significant temperature inversion at that height.

An interesting and unique sequence in this dataset occurs where a large PDC was captured in FLIR imagery taken by the IG around 0250 (Fig. 9). The infrasound power levels and jetting taper off rapidly around 0245 and the main plume detaches from the vent soon after. Even though infrasonic power levels decrease after the typical jetting signal ends at 0245, significant eruptive activity continues as numerous PDCs descend into local communities (Barba et al., 2006). This is coincident with the time the infrasound power levels decrease and a change in the frequency content occurs. Fig. 9a shows a comparison of the power spectral density (PDF) during a period of intense jetting with a sustained lava and ash column (July 15 0200–0207) vs. that during the collapsed column only portion (July 15 0248–0255). The jetting spectrum between 0200 and 0207 is typical of that at Tungurahua (Matoza et al., 2009) and during the main jetting phase of this eruption: July 14 2245–July 15 0230. This period also coincides with a sustained ash column. The spectrum following 0245 is roughly similar to the typical jet spectrum below 0.5 Hz, but has a sharper roll-off in the acoustic energy above 0.5 Hz (Fig. 9a). This is true of the entire spectrum between 0245 and 0315. Numerous PDCs were reported between 0315 and 0540 (Barba et al., 2006) with only a minor ash plume being driven by the PDCs. Activity at the vent during this period as captured by the FLIR camera is characterized by dense PDCs starting just above the vent and occurring in pulses. No large vertical plume is visible in the FLIR or satellite imagery, thus the acoustic

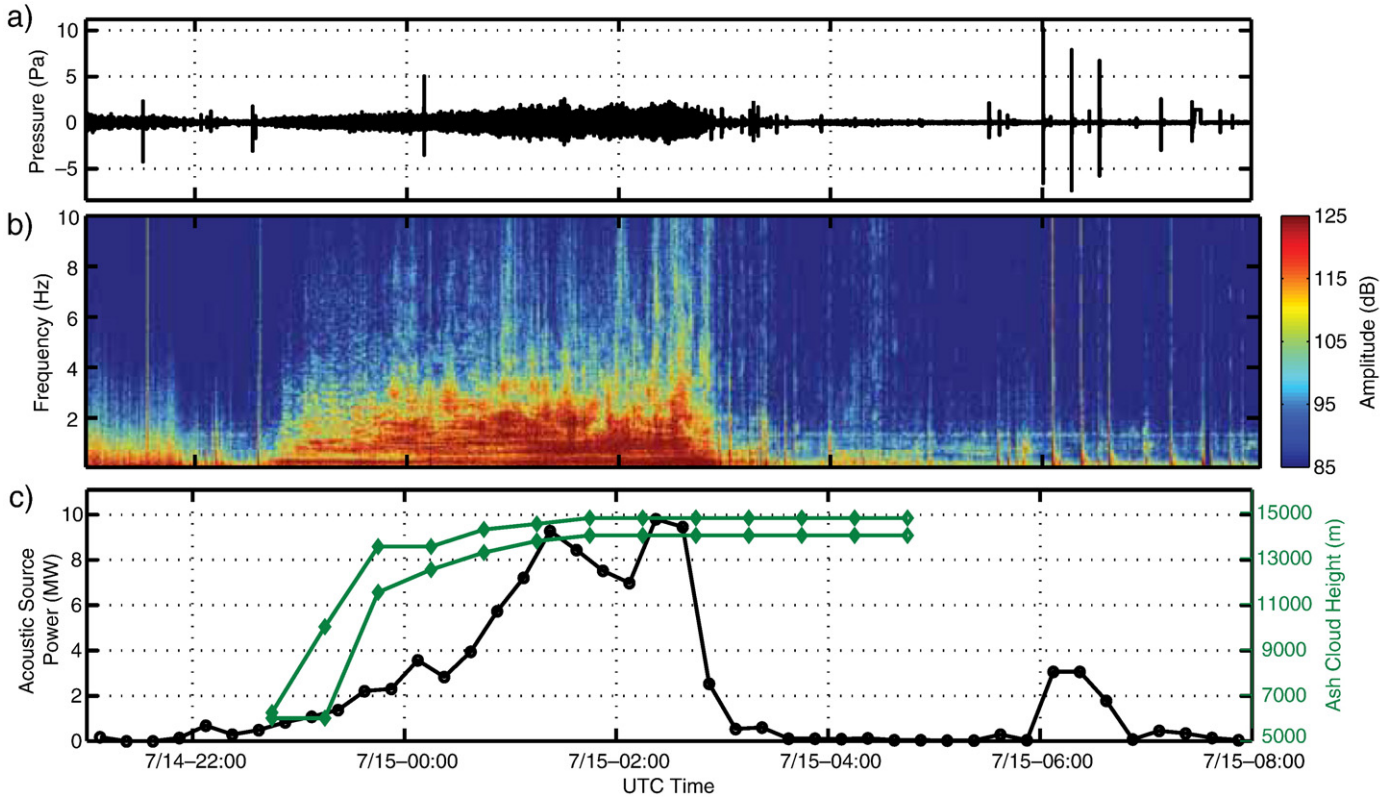

Fig. 8. July 14, 2006 a) raw waveform, b) spectrogram, and c) acoustic power (black line) and ash cloud height (green). The two ash cloud heights given are maximum and minimum, as derived from satellite imagery. Acoustic power broadly correlates with ash cloud heights.

source is likely within or near the crater. Infrasonic power levels decrease until 0540 and the spectrum retains a similar shape with a single dominant spectral peak around 0.25 Hz. Energetic explosions occur after ~0500 UTC, coincident with the appearance of a small ash cloud below 8 km, but no obvious correlations with PDCs or other activity are apparent. Remarkably, the steady 1.4 Hz tremor resumes at ~0315 and continues unabated. These PDC signatures will be addressed in more detail in Section 5.4.

4.4. August 16–17, 2006

On August 16–17, 2006 the most destructive and energetic eruption in Tungurahua's recent history occurred. Over 30 PDCs were observed (Barba et al., 2006), and the estimated DRE for this eruption is $\sim 2\times10^7$ m^3 (Arellano et al., 2008) and SO_2 emitted was over 35,000 tons (Carn et al., 2008). We estimate the eruption to be a VEI 4, primarily from the ash height (>24 km) and extended duration

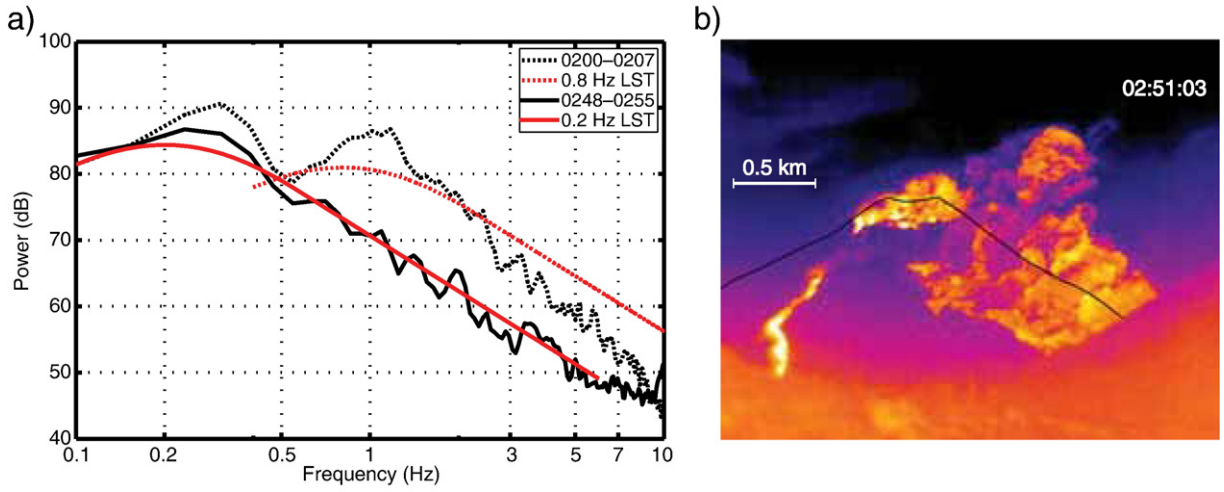

Fig. 9. PSD comparison for sustained vs. collapsed columns. a) Selected PSDs for July 15, 2006. The dashed black line is the spectrum during a time period of sustained jetting with a vertical ash and gas column above the vent. The dark black line indicates the spectrum during a period where the column has collapsed to feed PDCs. The red lines indicate the LST spectrum centered at different frequencies. Note there is no "notch" in the spectrum for the PDC period, only a single peak centered at ~0.25 Hz. b) FLIR image from July 15 02:51:03 UTC showing a large PDC descending the volcano and no sustained vertical column. This time period coincides with the single-peaked spectrum (black line) in a).

(~11 h). After a lull in activity following the July 14 eruption, activity at Tungurahua increased in the days preceding the August 16–17 eruption. A large bulge on the N flank of the volcano grew between August 11 and 16, and local authorities evacuated residents. A M_b 4.7 regional earthquake occurred ~60 km southeast of Tungurahua at August 16 0516, and this may have disrupted the volcano's plumbing system (Barba et al., 2006). Fig. 10 shows the raw waveforms (a), spectrogram (b), and acoustic power and ash heights (c) for the eruption.

On August 16 1930 the acoustic signal emerges gradually, and its spectrum is concentrated below ~2 Hz. This continuous tremor-like activity was noted to produce a steam-rich and ash-poor plume by the IG observers (Barba et al., 2006). The first ash plume is observed in satellite imagery at 2015 at a height of ~6–7 km, and remains at this height until ~0215 on the 17th. Acoustic power between 1930 and 2200 is fairly steady between 0.2 and 0.87 MW. After 2200 the spectrum becomes more broadband and jet-like. The peak-to-peak amplitudes of the infrasound signal are continuous at ~2 Pa, with power levels between ~1.1 and 2 MW. The IG reports the activity around 2200 resembles the onset of the July 14 eruption, with small PDCs, increased "roars" from the volcano, and a 100–200 m high lava fountain (Barba et al., 2006).

The acoustic jetting decreases slightly between 0000 and 0100. At 0115 the plume is observed to increase in width, length, and intensity; coincident with a marked increase in acoustic power between 0100 and 0200 to 7.5 MW. Local reports indicated a lava fountain to 800 m above the vent and numerous pyroclastic flows during this period (Barba et al., 2006). The plume top is still roughly at the same height (7.25 km).

Between 0200 and 0230 the acoustic power decreases slightly, followed by a significant increase to 12.8 MW at 0300, the highest recorded power from Tungurahua at that point. Broadband jetting and some explosions are apparent, although the explosions are difficult to discern within the constant ~5 Pa peak-to-peak jetting. Note the noticeable notch in the infrasound spectrum between ~0.35 and 0.9 Hz typical of the jet noise at Tungurahua during the study period (Matoza et al., 2009). Incandescent blocks, the ash column, "roars", and explosions were reported in the nearby towns of Riobamba (31 km) and Ambato (32 km). The observed ashfall during this period was similar to that during the paroxysmal phase of the July 14 eruption and numerous PDCs were observed (Barba et al., 2006). The ash plume increases in length and width, and rises to a height of 13.25 km at 0315.

Between 0330 and 0430 elevated activity continues and acoustic power is between 7 and 10 MW. At 0415 a substantial increase in the lateral dimensions in the ash cloud is apparent, and the height is estimated up to 17.5 km. The acoustic power increases slightly at 0400, but the change is not substantial and the power is similar to levels observed earlier. Between 0400 and 0500 the lava fountain is observed to stabilize and rise to a height of ~1.5 km with continued PDCs (Barba et al., 2006).

At August 17 0430 acoustic and eruptive activity declines substantially. An energetic Vulcanian explosion soon follows at 0436 UTC and signals the reactivation of the eruption. Intense acoustic activity continues for the next 1 h (~3–7 MW), and both the power levels and spectrum are similar to those recorded earlier (broadband jetting, notch in the spectrum, etc.). Unfortunately, there are no satellite observations of the ash plume during this period due to a satellite eclipse.

The paroxysmal phase of the eruption begins at ~0530 and continues until 0620. Acoustic power levels increase to their highest level (30 MW) and the jetting spectrum shifts to a lower frequency

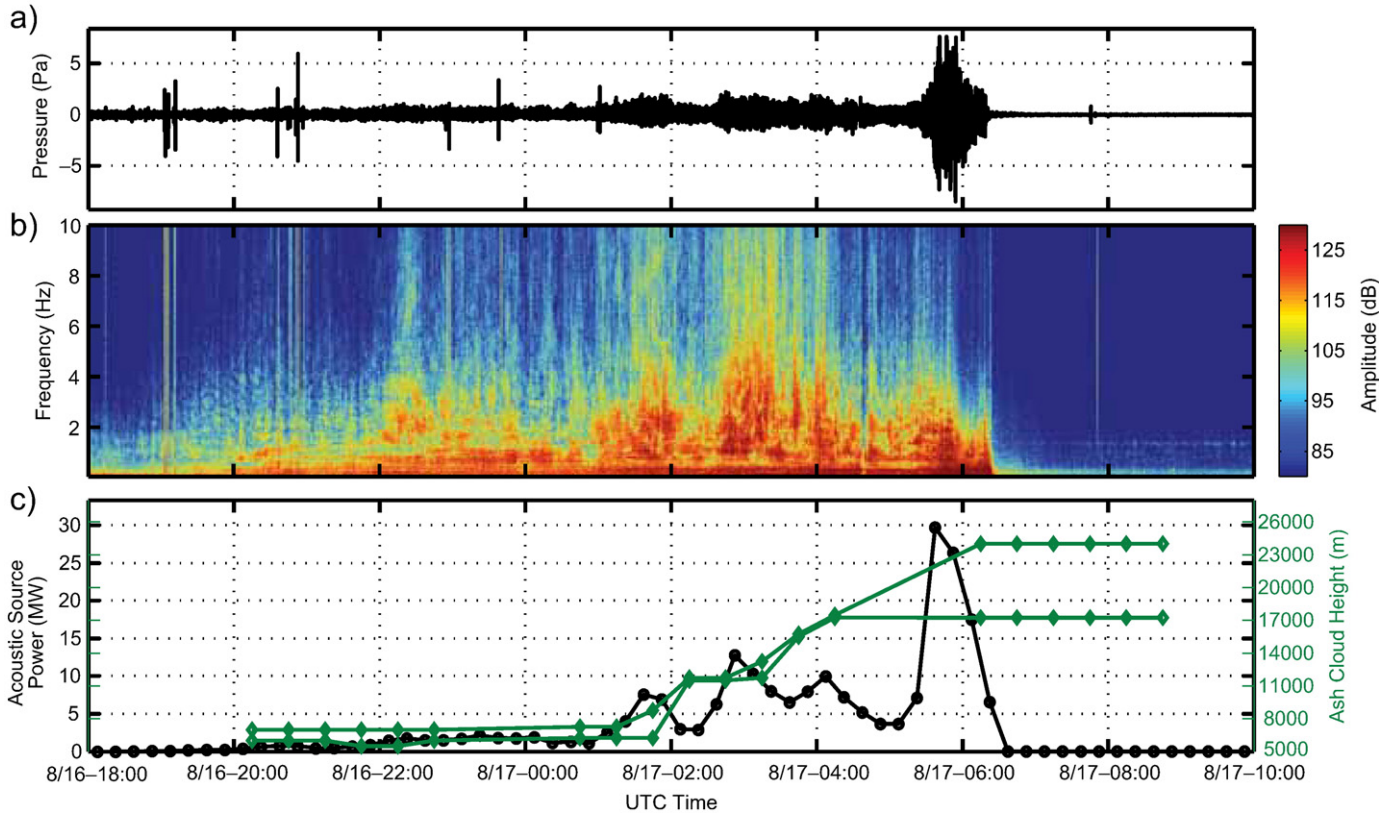

Fig. 10. August 16, 2006 a) raw waveform, b) spectrogram, and c) acoustic power (black line) and ash cloud height (green). The paroxysmal Plinian phase of the eruption begins around August 17 0600 UTC, where the ash height goes up to ~26 km. The green lines represent the minimum and maximum estimated ash cloud heights.

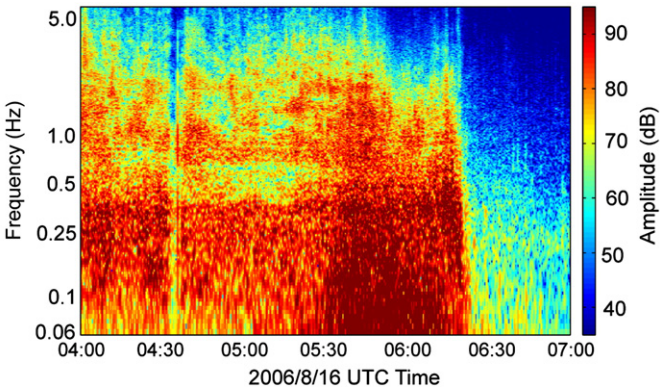

Fig. 11. August 16, 2006 spectrogram between 0400 and 0700 UTC. The dominant frequency of the jetting shifts to a lower frequency after ~0530, coinciding with a Plinian ash column. The eruption ends at ~0620.

(Garces et al., 2008; Matoza et al., 2009) (Fig. 11). The dominant frequency of jetting is now below 0.1 Hz, and although the instrument response has been corrected it is not completely resolved by our sensors as it lies outside the passband. However, it is clear that there is a significant shift in the spectrum. The peak-to-peak amplitude is ~16 Pa (Fig. 10a), a remarkably energetic signal at 37 km from the source. At 0615, the first satellite image after the data gap reveals a large circular plume (156×134 km) has risen to ~24 km, indicative of a Plinian ash column penetrating the stratosphere. The lava fountain was observed to be an astounding 6 km above the vent at this time, and numerous PDCs and heavy local ashfall occurred. Over 40% of the IG monitoring network was destroyed during this phase (Barba et al., 2006). After 0620 the infrasound power levels and eruptive activity drop off sharply to low levels. Remarkably, as after the July eruption, background 1.4 Hz tremor resumes at ~0730, seemingly unaffected by the cataclysmic eruption.

4.5. January 10–11, 2008

Intense Strombolian activity occurred between December 2007 and early February 2008. We select January 10–11 as a case study due to the heightened activity typical of this period and relative lack of meteorological clouds necessary for identifying ash clouds. Fig. 12 shows the raw waveforms (a), spectrogram (b), explosions, acoustic power and ash height (c) for January 10–11, 2008.

During these two days 428 Strombolian explosions are detected, and occur at a rate up to 32/h. The detected explosions are indicated by the red dots on top of Fig. 12c. The explosions peak pressure ranged between ~0.06 and 2.91 Pa, with most of them relatively small below ~0.35 Pa. Similarly, energy ratios range between 0.0012 and 3.32 with the mean at 0.06. The reduced number of detected explosions between ~1700 and 2200 on both days is due to the increased wind noise reducing the S/N and thus detection capability. No periods of energetic tremor or jetting occur during this period, although the background 1.4 Hz tremor was intermittently active. Despite the high number of explosions, only three low-level ash clouds were detected (Fig. 12c). The January 11 0315–0645 ash cloud is coincident with an increased rate of explosions and acoustic power. However, other periods of increased explosion energies and rates did not produce detectable ash clouds (e.g. January 10 0300–0600, January 11 2230). Similar to the May 2006 sequence, the explosions here are primarily gas-rich and produce little ash. The IG reports incandescent blocks are again erupted by the more powerful explosions, but significant fragmentation and ash emissions does not occur. The amplitudes and

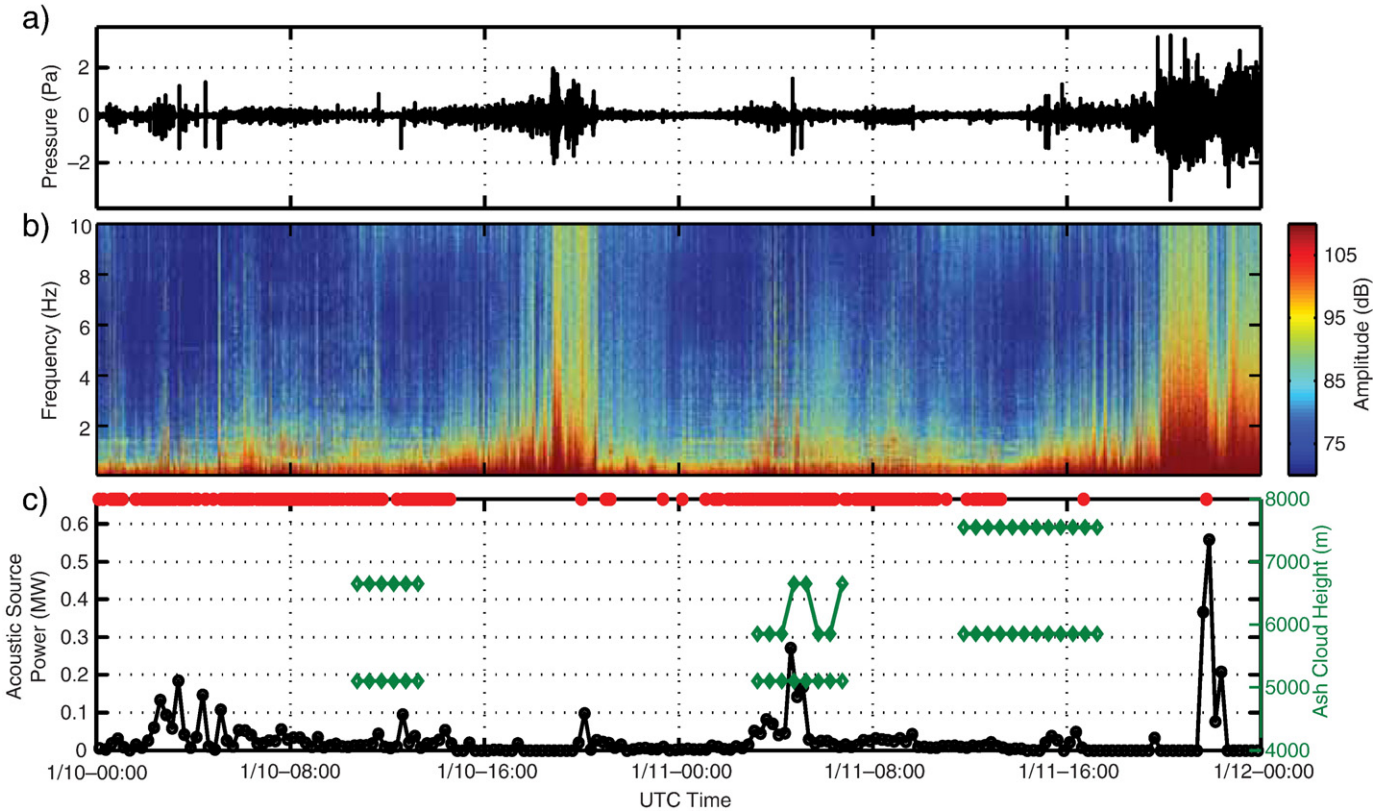

Fig. 12. January 10–11, 2008 a) raw waveform, b) spectrogram, and c) acoustic power (black line) and detected explosions (red dots). Numerous Strombolian–type explosions were detected throughout these two days, but no significant ash plumes were detected. Wind noise dominates the spectrogram during ~1900–2300 UTC.

energy of the explosions are smaller than the May sequence, although the rate and quantity are higher here.

4.6. February 6, 2008

After at least a month of escalating activity and numerous warning signs of an impending eruption, a Vulcanian–Subplinian eruption occurred at Tungurahua on February 6, 2008. This eruption was notable in that the autonomous ASHE monitoring and notification system was running and had been tuned using the July and August 2006 eruptions. Also noteworthy was the fact that rather than a sustained eruption for >4 h (July and August 2006), the February 6, 2008 eruption had numerous pulses of activity over 10.5 h, allowing easier correlations between changes in eruptive activity and its manifestations in the infrasound and satellite data. In the following detailed chronology of eruptive activity, we list selected detections and automatic notifications made by the ASHE project and split the eruption into four phases based on satellite and infrasound observations. Fig. 13 shows the raw waveforms (a), spectrogram (b), and acoustic power and ash height (c). ASHE energy and explosion notifications are also indicated by red and brown lines, respectively, in Fig. 13c.

The eruption began gradually on February 6. Numerous explosions occurred during the first part of the day, all of them with an energy ratio less than 1. This type of activity is very similar to that of January 10–11, 2008 and the days preceding this eruption. At ~0300 acoustic tremor begins, and the spectrum resembles low-level jetting. At 0415 the jetting becomes more continuous and the power levels rise. Similar to that of the July 14, 2006 and August 17, 2006 eruptions, there is a notch in the jetting spectrum between ~0.35 and 0.9 Hz. Poorly constrained PDCs were also reported b the IG. The majority of the signal is concentrated between ~0.1 and 2 Hz. At 0430 the ASHE acoustic energy notification threshold of 1×10^8 J is exceeded. A notification of elevated acoustic energy is sent to the VAAC and IG at 0434 UTC. The notification latency includes ~4 min for the data to be recorded, sent to Canada via satellite, forwarded to Hawaii via internet, and processed by the autonomous ASHE algorithms. Adding the acoustic travel time of ~1.8 min, the notification was sent ~5.8 min from the actual time of volcanic activity onset at Tungurahua, which is close to the 5 minute latency goal of the ASHE project.

At 0435, the calculated acoustic energy for the past hour increases to 4.41×10^8 J, and the 15 min power level is ~1 MW. Because the energy level has more than doubled, another email alert is sent out notifying of this change in eruptive activity. The first plume is observed in satellite imagery at 0445, and has a modest but still potentially hazardous height of ~6–7 km. The jetting decreases over time and lowers by 0515. This is coincident with the plume appearing detached from the summit in 0515 satellite image. This sequence is referred to as phase 1.

After a decrease in the acoustic power, the energetic jetting returns around 0540, beginning phase 2. The jetting continues until 0655 and the maximum acoustic power is 1.27 MW. The jetting is more broadband in phase 2 than in phase 1, although both have the characteristic notch in their spectrum. The phase 2 plume is first imaged at 0545 at a height of 6–8.4 km, increasing in width and length until 0645. The plume's volumetric increase is consistent with the increased acoustic jetting during this period. A large explosion occurs at 0626 ($E_r=13.83$, $P_p=3.85$ Pa). This explosion surpasses the explosion energy threshold and causes an email notification. Although the jetting decreases temporarily between ~0655 and 0700, it returns between 0700 and 0830 until phase 2 ends. The spectral structure for this time period is different than earlier in phase 2, as the higher frequencies (>2 Hz) show more variability. Power levels peak around

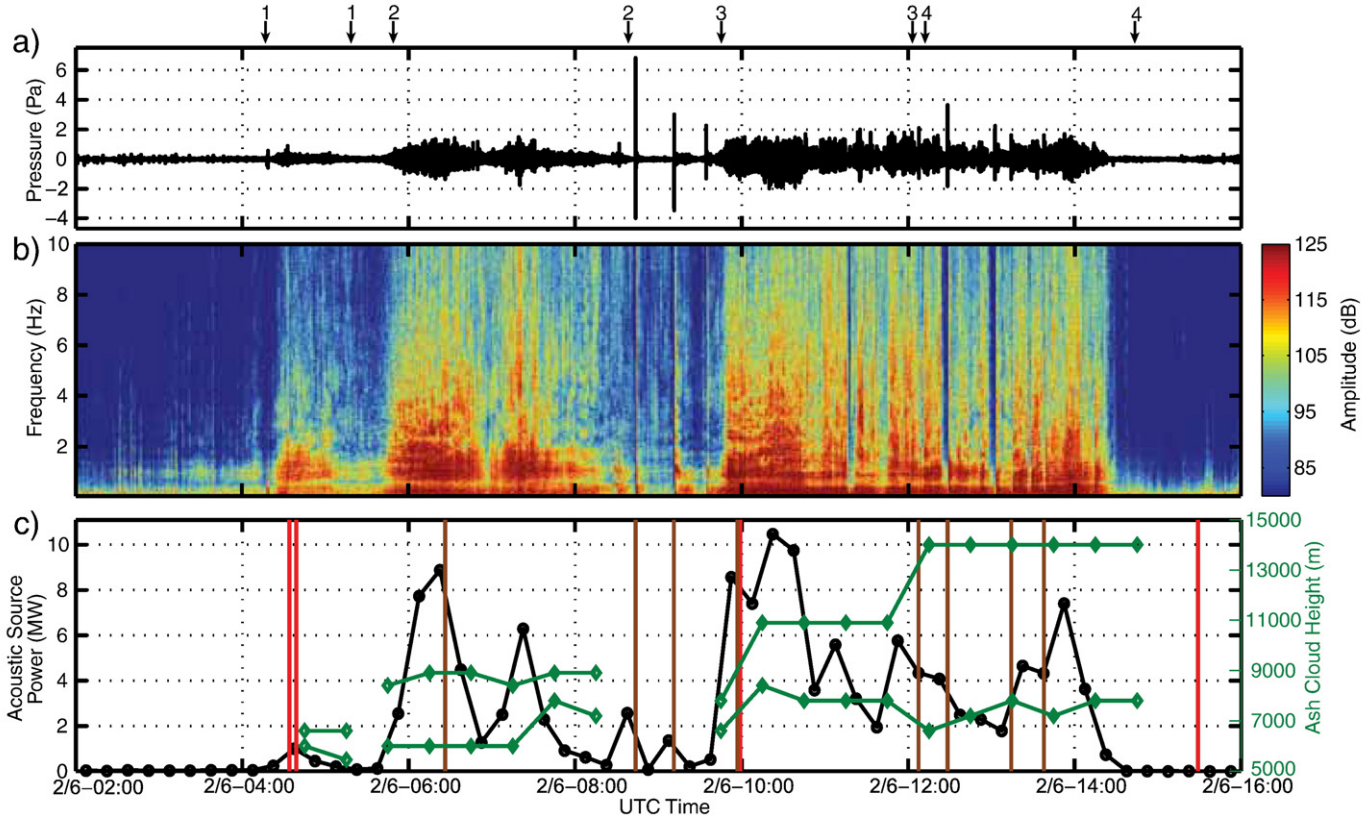

Fig. 13. February 6, 2008 a) waveforms, b) spectrogram, and c) acoustic power (black line) and ash cloud height (green). Red lines in c) indicate the automatic ASHE acoustic energy notifications sent to the VAAC. Brown lines in c) denote ASHE explosion notifications. The ASHE system notified the onset, escalation, and cessation of the major eruption. Arrows above a) indicate four eruption pulses referred to in text.

6.3 MW. Although the timing is difficult to discern due to missing images, the plume has detached from the summit by 0915. The infrasound power levels drop sharply from 0745 to 0900, except for two large explosion recorded at 0843 ($E_r = 96.0$, $P_p = 13.2$ Pa) and 0911 ($E_r = 35.6$, $P_p = 7.99$ Pa). These explosions occurred during a quiescent period where only small tremor or jetting was occurring, and no significant discrete thermal plume was produced from the explosion. However, the large energy ratios (>5) triggered an explosion email notification. For the first time during this eruption, harmonics are present in the spectrum between ~0800 and 0815 in both the explosion signals, reminiscent of the May 12 explosions (Section 4.2).

Phase 3 begins with the most acoustically energetic portion of the eruption between 0945 and 1115. The infrasound signal is broadband, constant, has the typical jet spectrum, and the peak power level is 10.5 MW. The 0945 GOES image shows a new plume up to 7 km attached to the summit which increases in width and height (10.9 km) until 1145. A 2 km high incandescent jet and numerous PDC are observed. Even though the last energy level notification was sent to the VAAC about 5.5 h earlier (0439), the acoustic energy has stayed above the energy level of the previous notification for each 5 minute update. For this reason no updated notification was sent out. At 0955 the energy level more than doubles from its previous value to 4.69×10^9 J and a new automatic notification is sent.

Although the plume stays attached to the summit during the rest of the eruption, the jetting decreases abruptly at 1115 for the next ~5 min. Between 1120 and 1205 phase 3 continues with two somewhat less energetic jetting pulses. These pulses are still significant with power levels between 1.9 and 5.8 MW. The plume decreases in width and length during these jetting pulses but remains attached to the summit.

Phase 4 lies between 1215 and 1430 and consists of at least seven distinct jetting pulses. The duration and frequency content of the jetting pulses varies slightly from pulse to pulse, but each is fairly similar in that they are preceded by a short period of quiescence, followed by an explosion, and then the typical jet noise spectrum. Four of these explosions triggered an explosion notification email: 1207 ($E_r = 7.38$, $P_p = 3.84$ Pa), 1228 ($E_r = 30.94$, $P_p = 8.76$ Pa), 1314 ($E_r = 6.26$, $P_p = 2.93$ Pa), and 1337 ($E_r = 5.69$, $P_p = 3.21$ Pa). In total 43 explosions are clearly detected during phase 4. Infrasound power levels oscillate somewhat during this phase, reaching a peak of 7.4 MW between 1345 and 1400. Numerous PDCs occurred during this phase and tephra fall to 3 cm was reported (Barba et al., 2006). The plume appears attached to the summit during all of phase 4. However, the satellite image is cropped during this period and it is difficult to discern the maximum extent of plume. Further the sampling interval of the GOES data limits high temporal tracking of the plumes. Estimates from the VAAC put the top of the plume at 14 km during phase 4. The acoustic power tapers off after the last pulse and the volcano is quiet after 1430. After staying at an elevated level for ~10 h, the volcano's hourly energy level has decreased and a notification to that effect is sent out at 1529. The DC VAAC cites decreased seismic and infrasound activity in their advisory at 1633 UTC.

5. Discussion

5.1. Constraining silicic eruptions using infrasound

Increases in acoustic power (a possible proxy for jetting intensity) during the major, sustained eruptions at Tungurahua between 2006 and 2008 are broadly consistent with increases in ash cloud height. Two exceptions are August 17, 2006 0300–0415 and July 15, 2006 0130–0300. Possible changes in the vent diameter, atmosphere, or multiphase eruptive mix may be responsible for these inconsistencies. Increases in acoustic power also correlate well with total ash cloud extent, which may not be as susceptible to the aforementioned factors. The acoustic power, onsets, and durations for the February 6, 2008 eruption correlate well with the observed ash plumes. Each of the 4 phases of ash emissions correspond with distinct acoustic phases (Fig. 12). Thus, in contrast to previous acoustic observations at Tungurahua (Johnson et al., 2005), acoustic energy release during large sustained eruptions does appear to broadly scale with eruption intensity.

Ash emissions for all three major eruptions are coincident with the onset and cessation of infrasonic jet noise. For example, the jetting during the July 14 eruption (~4.75 h, July 14 ~2245–July 15 0230) correlates well with the total duration and timing of the satellite-derived ash emissions (Fig. 8). Jet noise is attributed to small and large scale turbulence interactions within the momentum driven jet itself (Tam, 1998), with the infrasonic jet noise at Tungurahua most resembling large scale turbulence (Matoza et al., 2009). The relative acoustic power radiated is a function of the variations in velocity and volume flux of the ejecting gas–ash mixture. Following Lighthill's acoustic analogy (Lighthill, 1954), acoustic multipole radiation levels are predicted to follow velocity power laws (Woulff and McGetchin, 1975). Although comparing acoustic power to jet velocity is an enticing subject (Vergniolle and Caplan-Auerbach, 2006; Woulff and McGetchin, 1975), the complex nature of multipole source radiation and propagation make this a challenging task (Garces et al., in review).

Changes in the infrasonic frequency content are also likely indicators of changes in eruptive/jetting activity and are not as dependent on propagation and source directionality. Two prime examples are the paroxysmal Plinian phase of the August 17 eruption and the collapsing column at the end of the July 14 eruption (Section 5.3). The addition of VLP energy on August 17 (Figs. 10,11) indicates a significantly large and energetic source, in this case a high velocity jet ejecting ash into the stratosphere (Garces et al., 2008; Matoza et al., 2009). The peak acoustic power of ~30 MW underestimates the total acoustic power, as this calculation only considers frequencies above 0.1 Hz. To further illustrate the extent of low-frequency energy, Fig. 14 follows the aforementioned method of calculating acoustic power (Section 3.3) but divides the data into octave bands between 0.0625 and 16 Hz. The peak acoustic power of 17 MW in the 0.0626–0.125 octave band during the paroxysmal stage of the eruption August 17 is extraordinary, and could serve as a clear discriminator for stratospheric ash injection. Further, the total acoustic power is on the order of ~50 MW during this time period, a remarkable amount. As outlined in Section 3.3, this energy is

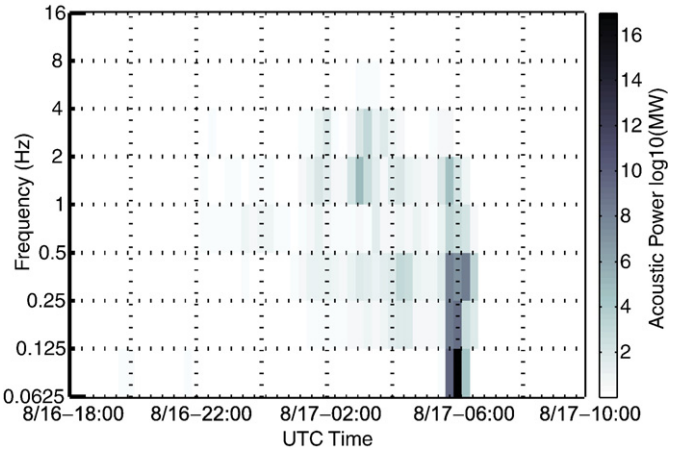

Fig. 14. Acoustic energy for the August 16, 2006 eruption. The acoustic energy was calculated in hour-long octave bands. The Plinian phase of the eruption is characterized by a significant amount of low-frequency (<.5 Hz) energy. Approximately 17 MW of power is detected in the 0.0626–0.125 octave band.

underestimated by at least a factor of 2 for a subaerial jet source, so the total radiated acoustic power in the 0.06–16 Hz band may be closer to ~0.1 GW near the source.

5.2. Generation of thermals

During the course of this experiment, large explosions were not indicative of significant ash emissions. No distinct thermals were detected in the satellite imagery or eye-witness observations from any of the May 12, 2006 explosions (Fig. 5). The Vulcanian explosions on February 6, 2008 were also not associated with distinct thermals, rather the sustained periods of jetting on this day were found to produce more significant ash (Fig. 13). The numerous Strombolian explosions from December 2007–February 2008 also only produced small to negligible ash clouds (Fig. 12). These assertions are broadly consistent with ground and satellite observations during other periods of the experiment as well. During the course of the experiment numerous explosion notifications were sent to the VAAC, but no clear correlation was found between energetic explosions and ash-laden thermals.

Of particular interest are the explosions that precede jetting and/or large eruptions. The July 14, 2006 2234 explosion signals the onset of jetting and ash emissions. The waveform and spectral features of this explosion are not significantly different than other explosions. The amplitude and energy are above average, but not extraordinary. The explosion preceding the jetting periods for the February 6, 2008 eruption have complicated waveforms, which could be due to complex source or propagation effects. The explosion at August 17, 2006 0436 also preceded jetting, but was not substantially different from other explosions during the experiment.

In order to transport ash to a significant altitude, sufficient momentum and then buoyancy must be imparted into the flow. Peak infrasonic amplitudes for explosions are related to the maximum overpressure, which occurs over a very short time period (<1 s). Longer duration momentum transfer (tremor and jetting) appears to be more conducive to significant ash injection. Multiple closely spaced explosions would put more energy into the system and increases the likelihood of a significant thermal (Sparks et al., 1997; Wilson et al., 1978). Although infrasound generating explosions at other volcanoes have produced significant thermals (e.g. Petersen et al., 2006; Vergniolle and Caplan-Auerbach, 2006), those at Tungurahua between 2006 and 2008 are possibly more gas-rich and ash-poor. Another consideration for the smaller impulsive events is atmospheric stability, which could either suppress or encourage plume rise. The larger eruption dynamics appear to be less vulnerable to local weather conditions due to their higher volume, momentum, and temperatures, which may overwhelm the ambient atmospheric state.

5.3. PDC generation

Volcanic column collapse occurs when the eruption column does not sufficiently entrain enough air to rise buoyantly. An increase in the degree of fragmentation or lithic material during an eruption would decrease the plume temperature and result in an increase in the time needed to transfer kinetic to thermal energy between the cooler particles and the hotter gas phase (Wilson et al., 1978; Woods, 1995), decreasing air entrainment. As an eruption progresses, erosion and widening of the conduit and crater would add lithics to the plume (Sparks et al., 1997; Woods, 1995). The 2006 Tungurahua eruptions significantly eroded and widened the crater to 300–400 m (Fig. 1b) and presumably the conduit as well. Further, widening of the conduit decreases the jet's ability to entrain enough air to rise buoyantly, thereby increasing the likelihood of column collapse (Sparks et al., 1997). In February 2008, Tungurahua's conduit was likely wider than in 2006, thereby making it more difficult to sustain a Plinian column, decreasing the ash heights, and increasing the likelihood of column collapse. This is consistent with the shorter duration of eruption pulses in the infrasound and satellite observations (Fig. 13).

Overpressured jets may also create annular flow in plumes and periodic column collapse without a change in the source conditions (Ogden et al., 2008). Higher vent overpressure on February 6, 2008 could have caused the intermittent column collapse and PDC generation (Fig. 13). Shock cells from overpressured jets could theoretically create broadband shock noise and screech tones (Tam, 1998) that could be recorded by our arrays. Some of the unexplained spectral structure above the 0.25 and 1 Hz peaks in the jet structure (Fig. 13) during the February eruption could be attributed to broadband shock noise, but the sharp spectral peaks from screech tones often produced by man-made, highly symmetric jets are not visible or likely.

5.4. Acoustics of sustained vs. collapsing columns

Jet noise at Tungurahua is thought to be produced by a combination of factors. Matoza et al. (2009) postulated that large scale turbulence (LST) interactions within the jet is a likely source due to the similarity of the Tungurahua jetting spectra with those established in controlled, man-made jets (Tam et al., 1996). The generally accepted model of LST noise generation consists of large turbulence structures (greater than the jet diameter) propagating as supersonic instability waves along the jet shear layer. The turbulence structures act similar to a "wavy-wall" radiating mach waves downstream (Tam, 1998). Note this mechanism requires a well-developed flow extending above the jet nozzle.

To better estimate the variability of the jet spectrum at Tungurahua, probability density functions (PDF) of the power spectral density estimates of jet noise are constructed in a manner similar to McNamara and Buland (2004). The PSD PDFs (Fig. 15) are constructed using beamformed 5 minute time windows of the RIOE data during the time periods encompassing the jetting during the case studies: July 14, 2006 2245–0245, August 16, 2006 2200–August 17, 2006 0630, and February 6, 2008 0415–1430 (Fig. 15a,b,c). The peak probability during the sequences is highlighted by the white dotted line. For comparison, a typical PSD of the Tungurahua background noise (July 29, 2006 0800–0900) is shown (Fig. 15a), including the typical 1.4 Hz tremor, as well as a typical spectrum from the Plinian portion of the August 16–17 eruption (Fig. 15b, black line). All three eruptions share similar characteristics, although the August and February jetting show higher variability. The typical jet spectrum at Tungurahua has two broad peaks at ~0.25 and ~1 Hz, with a notch in between (Figs. 9,15). The two spectral peaks at 0.25 and 1 Hz are clear for the July 2006 and Feb. 2008 eruption, but not as much for August 2006. Both spectral peaks are also apparent at the LITE array, suggesting neither is due to propagation effects. The jetting signals at RIOE vary from ~10–40 dB above the background noise, depending on the frequency.

The paroxysmal phase of the July 14, 2006 eruption allows a closer inspection of the jet noise sources. Although the exact sources are unresolved due to the complex nature of multiphase volcanic jets and recording limitations, the ~0.4–0.6 Hz notch in the jetting spectrum may be the result of gas–particle interactions not tested in typical laboratory experiments or simply the space between two separate noise sources with jet-related signatures (Matoza et al., 2009). The spectrum after the column collapses (after July 15 ~0245) shows only a single-peaked spectrum centered at ~0.25 Hz that fits the large scale turbulence (LST) similarity spectrum quite well (Fig. 9). Unlike the jetting signals studied by Matoza et al. (2009) and represented in Fig. 15, during the selected time window there is no sustained ash column, but rather a negatively buoyant mixture feeding numerous PDCs. The "wavy-wall" analogy extending above the vent for LST does not seem to be present for this period, unless a purely gaseous jet has decoupled from the particle laden PDC. However, a gaseous jet above

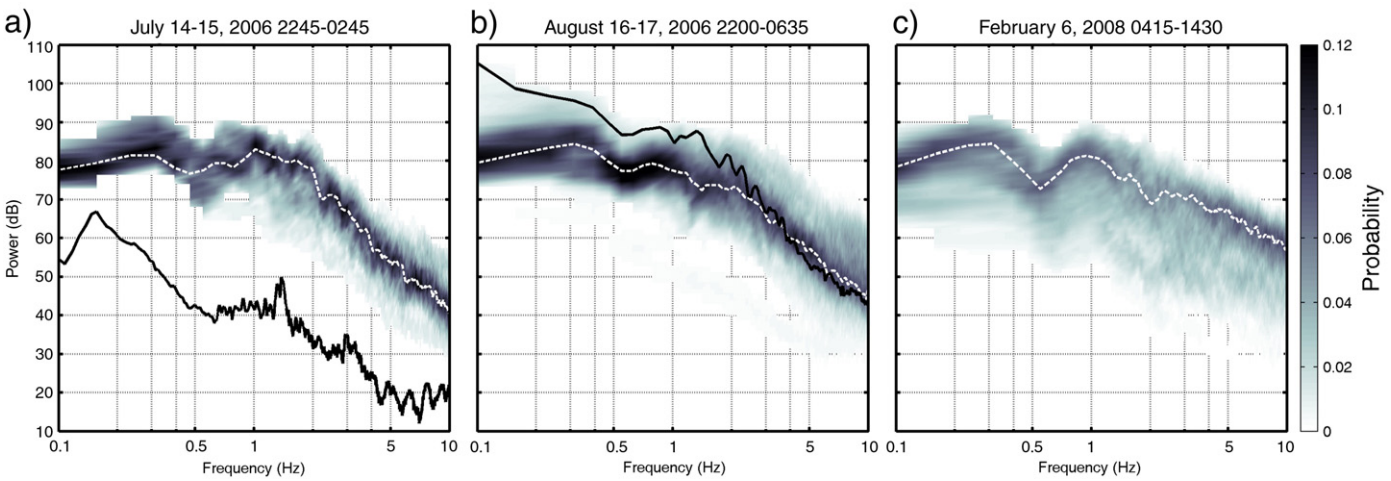

Fig. 15. Power spectral density probability density functions comparison for the three largest eruptions. Five minute long spectra are calculated and shown for a) July 14, 2006 2245–0245 UTC (4 h), b) August 16, 2006 2200–0630 UTC (8.5 h), and c) February 6, 2008 0415–1430 UTC (10.25 h). White lines indicate the peak probability. The black line in a) is typical of the background tremor at Tungurahua and is selected from July 29, 2006 0800–0900 UTC. All three eruptions have fairly typical broadband spectra with two spectral peaks at ~0.25 and 1 Hz and are well above the background noise at all frequencies. The black line in b) shows the spectrum between August 17, 2006 0545 and 0550 UTC, typical of the Plinian phase of the eruption. Note the Plinian spectrum has much lower frequency energy. The sensor response begins to roll-off below 0.1 Hz.

the vent would likely be visible in the FLIR imagery. Because the single 0.25 Hz peak is still present during this period, different physical processes are likely responsible for the peaks in the typical Tungurahua jet spectrum. The higher frequency (~1 Hz) peak may thus be associated with a well-developed jet (e.g. LST from a wavy-wall), while the 0.25 Hz peak may be due to a different source. The PDC itself is a turbulent noise source (Ripepe et al., 2009; Yamasato, 1997), but is unlikely due to the persistence of the spectral peaks throughout the three large eruptions (Fig. 15) and the fact that PDCs were not generated during the entirety of jet noise recording.

Most jet noise models are concerned with turbulence interactions downstream of the nozzle. Turbulence is a relatively inefficient noise producer due to its quadrupole radiation (Lighthill, 1954), but interactions of flow with solid surfaces can produce more efficient noise (Howe, 1998). The addition of solid surfaces interacting with the flow can substantially affect the noise produced by 1) promoting the conversion of flow energy to acoustic energy, 2) introducing reverberation effects that can feed back to the flow, and 3) creating sound-generating flow features such as vortex shedding and edge tones (Wang, 2005). The substantial broadband noise peak at 0.25 Hz produced during the entirety of the three large eruptions of 2006–2008 and documented during the generation of a large PDC on July 15, 2006, requires a continuous broadband acoustic source. One possibility for the 0.25 Hz spectral peak may be turbulent interactions of the flow with surrounding crater walls (Matoza et al., 2009; Woulff and McGetchin, 1975). The deep, heavily eroded summit crater at Tungurahua extends at least 100 m down from the crater rim, and is ~300–400 m wide (Fig. 1b). Jets emanating from volcanic conduits with pressure greater than atmospheric will decompress rapidly and interact with volcanic crater walls. The crater can both increase the jet velocity by providing additional upward thrust and affect the stability of the column (Woods and Bower, 1995). Jet interactions with the crater walls at Tungurahua are hypothesized as a possible source mechanism for the relatively steady 0.25 Hz infrasonic peak.

6. Conclusions

Two infrasound arrays deployed in Ecuador provide a continuous record of the activity at Tungurahua Volcano between 2006 and 2008. A system was set up to automatically detect significant volcanic activity and notify the VAAC of a possible aviation hazard. After two large eruptions in 2006 were used to refine the automated ASHE algorithms, the onset of the Subplinian February 6, 2008 eruption was detected and a notification was sent ~5.8 min after the acoustic onset. Acoustic energy from sustained, energetic eruptive activity at Tungurahua broadly scales with ash height and has a characteristic spectrum resembling a low-frequency form of jet noise. During the paroxysmal Plinian phase of the August 2006 eruption, the jet noise spectrum clearly shifts to low frequencies (below 0.1 Hz) and produces over 50 MW (5×10^7 W) of acoustic power. These high power levels suggest not only that the acoustic contribution to the total energy budget is not negligible, but also that the acoustic efficiency of volcanic processes may be higher than anticipated. Numerous short duration Strombolian and Vulcanian explosions were primarily gas-rich and did not produce significant ash clouds. A collapsed volcanic column during the July 2006 eruption has a unique infrasonic spectrum and may suggest a relationship between jet noise and column buoyancy. The interaction of the high velocity, unsteady, energetic jet with the crater walls is hypothesized as a potential source mechanism for low-frequency sound production and spectral modulation.

The ASHE proof-of-concept project has demonstrated that acoustic array monitoring of large volcanic eruptions at regional distances is not only viable, but also sufficiently mature to transition into operational volcano monitoring. In conjunction with other technologies such as remote sensing, infrasound can assist in providing low-latency notification of increased volcanic unrest and ash emissions, particularly for large eruptions. Further, it provides a remote sensing tool to study the dynamics of a variety of eruption styles. In order to validate and test the results presented here, the ASHE project is being extended to the global infrasound network of the International Monitoring System (IMS). In ongoing follow-up work, we are focusing on Subplinian to Plinian eruptions of the past decade consistently recorded by multiple IMS arrays.

Acknowledgements

The authors are grateful to the entire ASHE team for making this work possible, with special thanks to the Geological Survey of Canada for their technical and logistical support and to the dedicated staff of the Instituto Geofisico for their persistent and invaluable monitoring of Tungurahua. Patricio Ramon at the IG was exceptionally helpful in the preparation of this manuscript. Rene Servranckx at the Montreal VAAC and the helpful staff of the Washington DC VAAC provided invaluable feedback and assistance. Countless discussions with Robin Matoza help improve this work immensely. Sara McNamara helped with some of the ASHE algorithm development. Doug Drob graciously provided the atmospheric models. Helpful comments

from two anonymous reviewers greatly improved the manuscript. This work was made possible by the National Oceanic and Atmospheric Administration through University of Mississippi subcontract 09-09022.

References

Arellano, S.R., Hall, M., Samaniego, P., Le Pennec, J.-L., Ruiz, A., Molina, I., Yepes, H., 2008. Degassing patterns of Tungurahua Volcano (Ecuador) during the 1999–1006 eruptive period, inferred from remote spectroscopic measurements of SO_2 emissions. Journal of Volcanology and Geothermal Research 176, 151–162.

Barba, D., Arellano, S., Ramon, P., Mothes, P., Alvarado, A., Ruiz, G., Troncoso, L., 2006. Cronologia de los Eventos Eruptivos de Julio y Agosto del 2006 del Volcan Tungurahua, Resumenes extendidos de las 6th Jornadas en Ciencias de la Tierra. EPN-DG, Quito-Ecuador. pp. 177–180.

Cansi, Y., 1995. An automatic seismic event processing for detection and location; the P.M.C.C. method. Geophysical Research Letters 22 (9), 1021–1024.

Carn, S.A., Krueger, A.J., Krotkov, N.A., Arellano, S., Yang, K., 2008. Daily monitoring of Ecuadorian volcanic degassing from space. Journal of Volcanology and Geothermal Research 176 (1), 151–162.

DeFatta, D.J., Lucas, J.G., Hodgkiss, W.S., 1998. Digital Signal Processing: A System Design Approach. John Wiley, NY.

Fee, D., Garces, M., 2007. Infrasonic tremor in the diffraction zone. Geophysical Research Letters 34 (16).

Garces, M., Fee, D., Steffke, A., McCormack, D.P., Servranckx, R., Bass, H., Hetzer, C., Heldin, M., Matoza, R.S., Yepes, H., Ramon, P., 2008. Capturing the acoustic fingerprint of stratospheric ash injection. Eos, Transactions, American Geophysical Union 89 (40).

Garces, M., Fee, D. and Matoza, R.S., in review. Volcano Acoustics. In: S.A. Fagents, T.K.P.a. Gregg and R.C. Lopez (Editors), Modeling Volcanic Processes: The Physics and Mathematics of Volcanism. Cambridge Univ Press.

Green, D.N., Neuberg, J., 2006. Waveform classification of volcanic low-frequency earthquake swarms and its implication at Soufriere Hills Volcano, Montserrat. Journal of Volcanology and Geothermal Research 153 (1–2), 51–63.

Hall, M.L., Robin, C., Beate, B., Mothes, P., Monzier, M., 1999. Tungurahua Volcano, Ecuador; structure, eruptive history and hazards. Journal of Volcanology and Geothermal Research 91 (1), 1–21.

Ham, F.M., Leeney, T.A., Canady, H.M., Wheeler, J.C., 1999. Discrimination of volcano activity and mountain associated waves using infrasonic data and a backpropagation neural network. Applications and Science of Computational Intelligence Ii 3722, 344–356.

Howe, M.S., 1998. Acoustics of Fluid–Structure Interactions. Cambridge University Press. 560 pp.

Johnson, J.B., 2003. Generation and propagation of infrasonic airwaves from volcanic explosions. Journal of Volcanology and Geothermal Research 121 (1–2), 1–14.

Johnson, J.B., Ruiz, M.C., Lees, J.M., Ramon, P., 2005. Poor scaling between elastic energy release and eruption intensity at Tungurahua Volcano, Ecuador. Geophysical Research Letters 32 (15), 15.

Johnson, J., Aster, R., Jones, K.R., Kyle, P., McIntosh, B., 2008. Acoustic source characterization of impulsive Strombolian eruptions from the Mount Erebus lava lake. Journal of Volcanology and Geothermal Research 177 (3), 673–686.

Kumagai, H., Yepes, H., Vaca, M., Caceres, V., Nagai, T., Yokoe, K., Imai, T., Miyakawa, K., Yamashina, T., Arrais, S., Vasconez, F., Pinajota, E., Cisneros, C., Ramos, C., Paredes, M., Gomezjurado, L., Garcia-Aristizabal, A., Molina, I., Ramon, P., Segovia, M., Palacios, P., Troncoso, L., Alvarado, A., Aguilar, J., Pozo, J., Enriquez, W., Mothes, P., Hall, M., Inoue, I., Nakano, M., Inoue, H., 2007. Enhancing volcano-monitoring capabilities in Ecuador. Eos, Transactions, American Geophysical Union 88 (23), 245–246.

Le Pichon, A., Vergoz, J., Blanc, E., Guilbert, J., Ceranna, L., Evers, L., Brachet, N., 2009. Assessing the performance of the International Monitoring System's infrasound network: geographical coverage and temporal variabilities. Journal of Geophysical Research-Atmospheres 114.

Lighthill, M.J., 1954. On sound generated aerodynamically. II. Turbulence as a source of sound. Proceedings of the Royal Society of London. Series A 222, 1–32.

Marchetti, E., Ripepe, M., Harris, A.J.L., Delle Donne, D., 2009. Tracing the differences between Vulcanian and Strombolian explosions using infrasonic and thermal radiation energy. Earth and Planetary Science Letters 279 (3–4), 273–281.

Matoza, R.S., Hedlin, M.A.H., Garces, M.A., 2007. An infrasound array study of Mount St. Helens. Journal of Volcanology and Geothermal Research 160, 249–262.

Matoza, R.S., Fee, D., Garces, M.A., Seiner, J.M., Ramon, P.A., Hedlin, M.A.H., 2009. Infrasonic jet noise from volcanic eruptions. Geophysical Research Letters 36 (L08303).

McNamara, D.E., Buland, R.P., 2004. Ambient noise levels in the continental United States. Bulletin of the Seismological Society of America 94 (4), 1517–1527.

Ogden, D.E., Glatzmaier, G.A., Wohletz, K.H., 2008. Effects of vent overpressure on buoyant eruption columns: implications for plume stability. Earth and Planetary Science Letters 268 (3–4), 283–292.

Petersen, T., De Angelis, S., Tytgat, G., McNutt, S.R., 2006. Local infrasound observations of large ash explosions at Augustine Volcano, Alaska, during January 11–28, 2006. Geophysical Research Letters 33 (12).

Pierce, A.D., 1981. Acoustics — An Introduction to Its Physical Principles and Applications. McGraw-Hill, New York.

Ripepe, M., De Angelis, S., Lacanna, G., Poggi, P., Williams, C., Marchetti, E., Delle Donne, D., Ulivieri, G., 2009. Tracking pyroclastic flows at Soufrière Hills Volcano. EOS Transactions 90 (27). doi:10.1029/2009EO270001.

Ruiz, M., Lees, J.M., Johnson, J.B., 2006. Source constraints of Tungurahua Volcano explosion events. Bulletin of Volcanology 68 (5), 480–490.

Smithsonian, I., 2006. Tungurahua, Bulletin of the Global Volcanism Network (BVGN).

Sparks, R.S.J., Bursik, M.I., Carey, S.N., Gilbert, J.S., Glaze, L.S., Siggurdsson, H., Woods, A.W., 1997. Volcanic Plumes. John Wiley and Sons, New York. 574 pp.

Steffke, A., Fee, D., Garces, M. and Harris, A., in review. Identifying eruption chronologies, plume heights and eruption styles at Tungurahua Volcano: Integrating thermal infrared satellite and infrasound data. Journal Of Volcanology And Geothermal Research.

Sutherland, L.C., Bass, H.E., 2004. Atmospheric absorption in the atmosphere up to 160 km. Journal of the Acoustical Society of America 115 (3), 1012–1032.

Tam, C.K.W., 1998. Jet noise: since 1952. Theoretical And Computational Fluid Dynamics 10 (1–4), 393–405.

Tam, C.K.W., Golebiowski, M., Seiner, J.M., 1996. On the two components of turbulent mixing noise from supersonic jets. AIAA Pap 96, 1716.

Vergniolle, S., Caplan-Auerbach, J., 2006. Basaltic thermals and subplinian plumes: constraints from acoustic measurements at Shishaldin volcano, Alaska. Bulletin of Volcanology 68 (7–8), 611–630.

Vergniolle, S., Mangan, M., 2000. Strombolian and Hawaiian eruptions. In: Sigurdsson, H. (Ed.), Encyclopedia of Volcanoes. Academic Press.

Vergniolle, S., Brandeis, G., Mareschal, J.C., 1996. Strombolian explosions. 2. Eruption dynamics determined from acoustic measurements. Journal of Geophysical Research-Solid Earth 101 (B9), 20449–20466.

Wang, M., 2005. Computation of trailing-edge aeroacoustics with vortex shedding. Center for Turbulence Research Annual Research Briefs, pp. 379–388.

Waxler, R., Gilbert, K.E., Talmadge, C., 2008. A theoretical treatment of the long range propagation of impulsive signals under strongly ducted nocturnal conditions. Journal of the Acoustical Society of America 124 (5), 2742–2754.

Wilson, L., Sparks, R.S.J., T.C., H., N.D, W., 1978. The control of volcanic column heights by eruption energetics and dynamics. Journal of Geophysical Research-Solid Earth 83 (B4), 1829–1836.

Woods, A.W., 1995. The dynamics of explosive volcanic-eruptions. Reviews of Geophysics 33 (4), 495–530.

Woods, A.W., Bower, S.M., 1995. The decompression of volcanic jets in a crater during explosive volcanic-eruptions. Earth and Planetary Science Letters 131 (3–4), 189–205.

Woulff, G., McGetchin, T.R., 1975. Acoustic noise from volcanoes: theory and experiment. Geophysical Journal of the Royal Astronomical Society 45, 601–616.

Yamasato, H., 1997. Quantitative analysis of pyroclastic flows using infrasonic and seismic data at Unzen volcano, Japan. Journal of Physics of the Earth 45 (6), 397–416.